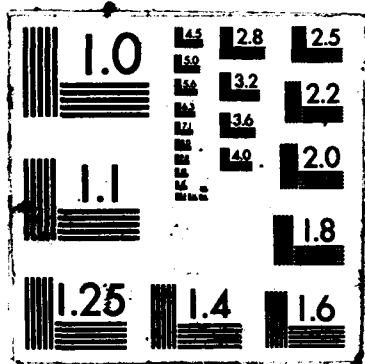


UNCLASSIFIED

F19626-86-C-0052

41

F/G 8/11



AD-A181 161

**LOCATION ESTIMATION
USING
REGIONAL ARRAY DATA**

by

Steven R. Bratt

Thomas C. Bache

SEMI-ANNUAL TECHNICAL REPORT NO. 1

Science Applications International Corporation
10210 Campus Point Drive
San Diego, California 92121

31 December 1986

Approved for Public Release; Distribution Unlimited

DTIC
ELECTE
S JUN 11 1987 **D**
E

AIR FORCE GEOPHYSICS LABORATORY
AIR FORCE SYSTEMS COMMAND
UNITED STATES AIR FORCE
HANSCOM AIR FORCE BASE, MA 01731

87

6

9

004

The views and conditions contained in the document are those of the authors and should not be interpreted as necessarily representing the official policies, expressed or implied of the Air Force Technical Applications Center or the U.S. Government.

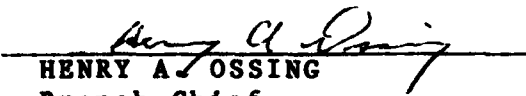
SPONSORED BY:
Defense Advanced Research Project Agency (DoD)
Defense Sciences Office, Geophysical Sciences Division
DARPA/DSO Signal Analysis and Identification Methods Program
DARPA Order No. 5307

Issued by:
Air Force Geophysics Laboratory Under
Contract No. F19628-86-C-0052

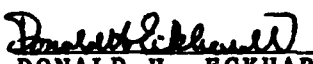
Principal Investigator: Dr. Thomas Bache (619) 458-2531

"This technical report has been reviewed and is approved for publication."


JAMES F. LEWKOWICZ
Contract Manager


HENRY A. OSSING
Branch Chief

FOR THE COMMANDER


DONALD H. ECKHARDT
Division Director

This report has been reviewed by the ESD Public Affairs Office (PA) and is releasable to the National Technical Information Service (NTIS).

Qualified requestors may obtain additional copies from the Defense Technical Information Center. All others should apply to the National Technical Information Service.

If your address has changed, or if you wish to be removed from the mailing list, or if the addressee is no longer employed by your organization, please notify AFGL/DAA, Hanscom AFB, MA 01731. This will assist us in maintaining a current mailing list.

Do not return copies of this report unless contractual obligations or notices on a specific document requires that it be returned.

UNCLASSIFIED

SECURITY CLASSIFICATION OF THIS PAGE

AD A181 161

REPORT DOCUMENTATION PAGE

1a. REPORT SECURITY CLASSIFICATION Unclassified			1b. RESTRICTIVE MARKINGS		
2a. SECURITY CLASSIFICATION AUTHORITY			3. DISTRIBUTION/AVAILABILITY OF REPORT Approved for Public Release; Distribution Unlimited		
2b. DECLASSIFICATION/DOWNGRADING SCHEDULE					
4. PERFORMING ORGANIZATION REPORT NUMBER(S) SAIC 87/1564			5. MONITORING ORGANIZATION REPORT NUMBER(S) AFGL-TR-87-0108		
6a. NAME OF PERFORMING ORGANIZATION Science Applications International Corporation		6b. OFFICE SYMBOL (If applicable)		7a. NAME OF MONITORING ORGANIZATION Air Force Geophysics Laboratory (LWH)	
6c. ADDRESS (City, State, and ZIP Code) 10210 Campus Point Drive San Diego, CA 92121			7b. ADDRESS (City, State, and ZIP Code) Hanscom Air Force Base, MA 01731		
8a. NAME OF FUNDING/SPONSORING ORGANIZATION DARPA		8b. OFFICE SYMBOL (If applicable) GSD		9. PROCUREMENT INSTRUMENT IDENTIFICATION NUMBER F19626-86-C-0052	
8c. ADDRESS (City, State, and ZIP Code) 1400 Wilson Blvd. Arlington, VA 22209			10. SOURCE OF FUNDING NUMBERS		
			PROGRAM ELEMENT NO. 62714E	PROJECT NO. 6A10	TASK NO. DA
11. TITLE (Include Security Classification) Location Estimation Using Regional Array Data					
12. PERSONAL AUTHOR(S) Steven R. Bratt and Thomas C. Bache					
13a. TYPE OF REPORT Semi-Annual Report #1		13b. TIME COVERED FROM 2/86 TO 8/86		14. DATE OF REPORT (Year, Month, Day) 12/31/86	
15. PAGE COUNT 66					
16. SUPPLEMENTARY NOTATION					
17. COSATI CODES			18. SUBJECT TERMS (Continue on reverse if necessary and identify by block number) Seismic Verification, Seismic Location, Seismic Array		
FIELD	GROUP	SUB-GROUP			
19. ABSTRACT (Continue on reverse if necessary and identify by block number) A location estimation procedure for locating regional seismic events with a network including arrays and single element seismometers is described. The method incorporates back-azimuth estimates, arrival time data and associated uncertainties into a generalized-inverse location estimate. The formulation is essentially that of Jordan and Sverdrup (1981) extended to incorporate azimuth data. This formulation allows the use of both <i>a priori</i> and <i>a posteriori</i> information about data uncertainties to compute confidence ellipsoids for the location estimates. This is important for obtaining realistic confidence ellipsoids for solutions based on few data. → next page					
20. DISTRIBUTION/AVAILABILITY OF ABSTRACT <input type="checkbox"/> UNCLASSIFIED/UNLIMITED <input checked="" type="checkbox"/> SAME AS RPT. <input type="checkbox"/> DTIC USERS			21. ABSTRACT SECURITY CLASSIFICATION Unclassified		
22a. NAME OF RESPONSIBLE INDIVIDUAL James F. Lewkowicz			22b. TELEPHONE (Include Area Code) (619) 377-3028		22c. OFFICE SYMBOL AFGL/LWH

Another important attribute of the Jordan and Sverdrup (1981) formulation is that it provides for a refinement of the confidence ellipsoid calculations as experience accumulates for events in a particular area, and this is an important element of our regional location estimation procedure. Small arrays like NORESS in Norway provide accurate estimates for the back-azimuth of regional phases. These azimuth data provide a strong constraint on the location for events detected by a small number of stations, including at least one array. The strength of the constraint depends on the geometry, and in some situations azimuth data are as important as arrival-time data. Synthetic examples illustrating this are given for a network including two arrays. Actual data from the NORESS array in southern Norway and the FINESA array near Helsinki, Finland are presented to demonstrate the use of the regional location procedure. There are independent locations from a local network for most of the events studied. Comparing one-array and two-array locations and their confidence ellipses with these independent locations provides a preliminary validation of our estimates of the (signal-dependent) *a priori* arrival-time and azimuth variances and demonstrates the effectiveness of our location procedure for a sparse network of regional arrays.

Table of Contents

INTRODUCTION	1
ESTIMATING LOCATIONS WITH SMALL DATA SETS	3
EXTENDING LOCATION SOLUTIONS TO INCLUDE AZIMUTH DATA	8
DESCRIPTION OF EXAMPLES	12
LOCATION SOLUTIONS	20
<i>Application to Synthetic Data</i>	21
<i>Application to Actual Data</i>	32
DISCUSSION	50
ACKNOWLEDGMENTS	52
REFERENCES	53

Accession For	
DTIS GRA&I	<input checked="" type="checkbox"/>
DTIC TAB	<input checked="" type="checkbox"/>
Unannounced	<input type="checkbox"/>
Justification	
By _____	
Distribution/ _____	
Availability Codes	
Dist	Avail and/or Special
A-1	



INTRODUCTION

The NORESS array, a 25 element, 3 km aperture array in Norway, (Mykkeltveit *et al.*, 1983) is designed for detecting regional signals from small events. The underlying motivation is the need for improved capabilities to monitor underground nuclear explosion testing down to very low magnitudes. The array design cannot be said to represent an entirely new concept, since the 'Geneva arrays' deployed in the 1960's were similar in many ways (e.g., Romney, 1985). However, the improved instrumentation and processing capability now available make it possible to more effectively use the data from small, dense, high frequency arrays.

Our focus in this paper is on the use of data from NORESS-type arrays to locate regional events. We anticipate a network that includes several of these arrays, along with single seismometer stations. The events of primary interest are small and detectable by only a few arrays (perhaps only one). Thus, our objective is to develop and test a regional event location estimation procedure which takes full advantage of unique characteristics of data from these arrays and which is suitable for a network including arrays and lower quality stations. For location estimation, the unique feature of the data from the NORESS-type arrays (aside from the low detection threshold) is that one can obtain quite accurate estimates of the azimuth of detected phases. Thus, we need a location estimation procedure which takes maximum advantage of this capability.

The NORESS data are now automatically processed (Mykkeltveit and Bungum, 1984) to produce a bulletin of regional seismicity that is quite good for a single station (Mykkeltveit, 1985). The locations are computed from Lg - Pn travel time and Lg azimuth. Thus, azimuth data are now used routinely. Our objective is to extend this idea by developing a formal inversion procedure that allows the incorporation of all useful data (from one or more arrays and stations) and that provides an estimate of the solution uncertainty. We are particularly concerned with the calculation of the confidence ellipsoid for the solution and evaluation of its validity as a measure of solution accuracy. Azimuth estimates play an important role, and with a single array no confidence ellipsoid estimate is possible without them. Parenthetically, we note that the confidence ellipsoid for a single array location estimate provides key information for associating signals from the same event recorded at different stations and arrays.

Several investigators have examined the utility of including azimuth measurements as constraints on event location. Early studies by Shlien and Toksoz (1973), Julian (1973), Gjoystdal *et al.* (1973) considered the use of azimuth estimates from arrays, but were primarily concerned with teleseismic data. Smart (1978) used Lg azimuth estimates to locate regional events, and the work of Rivers *et al.*, 1981 extended this study to incorporate these azimuths in formal location inversion procedures. However, their azimuth estimates were obtained from three-component stations and were much less accurate than those available from frequency-wavenumber (f-k) processing of NORESS-type array data. Thus, Rivers *et al.* concluded that their azimuth estimates were not very useful, which is quite different from our conclusion based on the accurate azimuth estimates available from NORESS-type array data.

The location algorithm used (and extended) in our work is that of Jordan and Sverdrup (1981), which was specifically designed to provide reasonable confidence bounds when the data are few. This is the situation of primary interest, so this algorithm is especially well-suited to our problem. The confidence bounds are functions of the solution residuals, *a priori* estimates for the data variances, and a parameter which weights their relative contribution. These data variances can to some degree be estimated from the data, and as empirical experience is accumulated, the weight applied to them can be increased.

In this study we begin by describing the location estimation procedure of Jordan and Sverdrup (1981) and our extensions to incorporate azimuth data. We demonstrate the major features with 'synthetic' data. We then consider solutions obtained with actual data from a single array (NORESS) and from two arrays. The second array, FINESA (Korhonen *et al.*, 1986), is smaller (10 elements) and is located near Helsinki. We examine both the location precision, expressed by the confidence ellipsoid, and the location accuracy, which can best be evaluated by comparing estimated locations with actual locations determined by independent methods.

The examples we present are relatively few, but illustrate all important aspects of the technique and the quality of the solutions obtained. Further, they demonstrate that our choice of algorithms to compute the arrival time and azimuth variances for particular phases and our initial choice of the parameters controlling the confidence ellipsoids appear to be appropriate. We also demonstrate how the parameters can be adjusted to reflect accumulated experience.

ESTIMATING LOCATION WITH SMALL DATA SETS

Most methods for the estimation seismic event hypocenters are based on variations of the method of Geiger (1910). The unknown solution $\underline{\hat{x}}$ is a vector with up to four elements: event latitude, longitude, depth, and origin time. (In our notation we will use \underline{x} to represent an estimate for $\underline{\hat{x}}$, and similarly for other variables). In conventional solutions the N observations are arrival times $\underline{t}(\underline{\hat{x}})$ of various phases at each station in the network. A theoretical estimate ($\underline{t}_c(\underline{x}_c)$) of the data is computed from a trial solution at \underline{x}_c and an assumed earth model. An estimate for the actual location $\underline{\hat{x}}$ is obtained by minimizing the residual vector:

$$\underline{r} = (\underline{t} - \underline{t}_c) . \quad (1)$$

Linearized versions of the equations relating \underline{t} to \underline{x} are obtained by expansion in a Taylor series about the trial hypocenter \underline{x}_c . Based on these equations, the residuals can be represented by:

$$\underline{r} = A \Delta \underline{x} \quad (2)$$

where A is an $N \times M$ system matrix of the partial derivatives of travel time with respect to \underline{x}_c . The $\Delta \underline{x}$ is a vector of perturbations from the trial solution toward a solution that minimizes \underline{r} .

It is assumed that each element of \underline{r} is a normally distributed random variable with zero mean and variance σ_i^2 . The σ_i are typically estimated *a priori*, and are represented by an "assigned" standard deviation, σ_i . Though the σ_i may adequately characterize the effects of approximately-random processes such as reading errors and small-scale variation in velocity structure, they may poorly account for sources of bias like station elevation and gross structural heterogeneity. The bias effects are typically handled by applying station corrections to the data or by computing joint or relative location solutions (e.g., Douglas, 1967; Jordan and Sverdrup, 1981).

The assigned variances are frequently used to weight the data and associated partial derivatives.

The assigned variance matrix is:

$$\underline{V}_d = \begin{bmatrix} \sigma_1^2 & 0 & 0 & \dots \\ 0 & \sigma_2^2 & 0 & \dots \\ 0 & 0 & \sigma_3^2 & \dots \\ \vdots & \vdots & \vdots & \ddots \end{bmatrix} . \quad (3)$$

If the elements of \underline{r} are independent and the ratios of the σ_i were assigned correctly, the assigned variance matrix \underline{V}_d is related to the actual variance matrix $\hat{\underline{V}}_d$ by:

$$\hat{\underline{V}}_d = \hat{s}^2 \underline{V}_d , \quad (4)$$

where \hat{s}^2 is the variance scale factor, to be discussed later. Of course, when the $\sigma_i = \hat{\sigma}_i$, that is, when the assigned variances accurately describe the scatter in \underline{r} , the \hat{s}^2 is unity. Weighting by the variances transforms the residual and system matrices:

$$\underline{r}_w = \underline{V}_d^{1/2} \cdot \underline{r} \quad (5)$$

$$\underline{A}_w = \underline{V}_d^{1/2} \cdot \underline{A}$$

As a result of (5), a relative decrease in the assigned standard deviation of a given datum increases the weight of that datum in determining the final solution.

If the trial solution (\underline{x}_t) is sufficiently close to the actual solution ($\hat{\underline{x}}$) for (2) to be linear, \underline{x} can be determined immediately by inverting (2) for $\Delta \underline{x}$, using any number of methods (see Aki and Richards, 1980). We use the generalized inverse technique:

$$\Delta \underline{x} = (\hat{\underline{A}}_w \underline{A}_w)^{-1} \hat{\underline{A}}_w \underline{r}_w, \quad (6)$$

where \bar{A}_w is the transpose of A_w and $()^{-1}$ denotes the matrix inverse. The new estimate of \underline{x} is $\underline{x}_c + \Delta \underline{x}$. Usually the problem is nonlinear, and several iterations are required before \underline{r}_w is minimized.

Estimation of confidence bounds on the final solution \underline{x} has been the topic of numerous studies (e.g., Flinn 1965, Evernden, 1969). We have adopted the Jordan and Sverdrup (1981) method which takes advantage of *a priori* knowledge about data uncertainties to permit reasonable estimation of the location confidence ellipse when few data are available. We will briefly review this procedure.

A general formula for points \underline{x}_e on the p percent confidence ellipsoid for solution \underline{x} is:

$$(\underline{x}_e - \underline{x})^T \underline{V}_x^{-1} (\underline{x}_e - \underline{x}) = \kappa_p^2, \quad (7)$$

where \underline{V}_x is an estimate for the parameter covariance matrix,

$$\underline{V}_x = (\bar{A}_w^T A_w)^{-1}. \quad (8)$$

The confidence coefficient κ_p^2 is:

$$\kappa_p^2 = M \hat{s}^2 F_p[M, N - M], \quad (9)$$

where F_p is the F statistic with M and $N - M$ degrees of freedom at the p percent confidence level. The \hat{s}^2 is usually not known, but has been traditionally been estimated *a posteriori* by the normalized sample variance, s_s^2 :

$$s_s^2 = \frac{|\underline{r}_w|^2}{N - M} \quad (10)$$

The error ellipse described by (7) through (10) is essentially that of Flinn (1965) and is incorporated into most widely used location algorithms such as HYPOINVERSE (Klein, 1978).

The s_s^2 from (10) is a satisfactory approximation of \hat{s}^2 only for large data sets ($N \gg M$). However, as N approaches M , the s_s^2 , the F_p , and therefore the dimensions of the confidence ellipsoid, become unreasonably large. Alternatively, both s_s^2 and the confidence ellipse can become unreasonably small when $|r_w|^2$ is near zero; a situation more likely when the number of data used is small. Evernden (1969) suggested an alternative approach which mitigates these problems. If one assumes the variances \hat{V}_d to be perfectly known *a priori*, then $\hat{s}^2 = 1$, and the confidence coefficient reduces to:

$$\kappa_p^2 = \chi_p^2 [M], \quad (11)$$

where χ_p^2 is the p percent chi-squared statistic with M degrees of freedom. But this estimate is incorrect to the extent that the \hat{V}_d are not perfectly known, and in many cases our estimate is rather poor.

The unique contribution of the Jordan and Sverdrup (1981) method is its incorporation of both *a priori* and *a posteriori* information about the data to derive location confidence bounds. Using Bayesian statistical theory, they rederive (9) and (10) and obtain the confidence coefficient:

$$\kappa_p^2 = M \hat{s}^2 F_p[M, K + N - M], \quad (12)$$

where the new effective *a posteriori* estimate for the variance scale factor \hat{s}^2 is given by:

$$s_e^2 = \frac{K s_K^2 + |r_w|^2}{K + N - M}, \quad (13)$$

The s_K^2 is an *a priori* estimate for \hat{s}^2 and can be determined from the normalized sample variances computed during a series of J location experiments:

$$s_K^2 = \frac{1}{J} \sum_{j=1}^J (s_s^2)_j. \quad (14)$$

K can be viewed as a measure of uncertainty in s_K^2 . Jordan and Sverdrup (1981) relate K directly to the standard deviation of the quantity $(1 / s_s)$ for the J experiments used to estimate s_K^2 . When $K = 0$, \hat{s}^2 is not known *a priori*, and it must be estimated from the data. In this case equation (13) reduces to (10). The dimensions of the resulting confidence ellipsoid depend only on the variance-weighted misfit between the observations and the solution (i.e., the Flinn (1965) solution). When $K = \infty$, \hat{s}^2 is assumed to be known perfectly *a priori*, i.e., $s_s^2 = \hat{s}^2$. In this case equations (12) and (13) reduce to (11), using $F_p[M, \infty] = \chi_p^2[M] / M$ (i.e., the Evernden (1969) solution). For intermediate values of K the dimensions of the confidence ellipsoid depend both on the solution residuals and the *a priori* assumptions about the data variances, with the weighting determined by the chosen K . For example, when $K = 1$ and 8, the implied standard deviations in $(1 / s_s)$ are about $\pm 60\%$ and 25% , respectively.

The use of this procedure for sparse network location estimation is straightforward. As more data are accumulated, area-specific values of s_K^2 are computed. If the assigned data variances have been estimated reasonable well, s_K^2 should be close to unity. Alternatively, the s_K^2 and residuals for individual types of data (i.e., P-waves at a particular station) can be used to re-adjust the variances so that s_K^2 moves toward unity. As the variances for data from events in a particular region become better understood, the standard deviation of $(1 / s_s)$, should decrease, and this is reflected by an increase in K . Thus, the accuracy of the "K-weighted" confidence ellipsoid (as we will refer to it throughout the text) improves with experience, even though the number of data used to locate individual events remains small.

EXTENDING LOCATION SOLUTIONS TO INCLUDE AZIMUTH DATA

The Jordan and Sverdrup (1981) location algorithm can easily be extended to include azimuth data. This is done by including additional rows in the residual (\underline{r}) and system (\underline{A}) matrices as follows:

$$\underline{r} = \begin{bmatrix} t - t_c \\ \cdot \\ \cdot \\ \alpha - \alpha_c \end{bmatrix} \quad (15)$$

$$\underline{A} = \begin{bmatrix} \frac{\partial t_1}{\partial x} & \frac{\partial t_1}{\partial y} & \frac{\partial t_1}{\partial z} & \frac{\partial t_1}{\partial T_o} \\ \cdot & \cdot & \cdot & \cdot \\ \cdot & \cdot & \cdot & \cdot \\ \cdot & \cdot & \cdot & \cdot \\ \frac{\partial \alpha_N}{\partial x} & \frac{\partial \alpha_N}{\partial y} & 0 & 0 \end{bmatrix} \quad (16)$$

Azimuth residuals are computed as the difference between the observed azimuth (measured clockwise from the north) and the azimuth from the station to the trial location. As before, the solution is obtained by minimizing the norm of \underline{r}_w , the normalized residual vector. The \underline{A} includes partials of azimuth with respect to cartesian coordinates x (easterly) and y (northerly). Figure 1a illustrates the change in α produced by a eastward change (δx^o , in radians) in event location from \underline{x}_o to \underline{x}_E . The station is initially Δ radians distant and α_e radians azimuth from the event. Side b is drawn from \underline{x}_E to side Δ to form two right spherical triangles. From spherical trigonometry, the change in azimuth at the station may be represented by:

$$\sin(-\delta\alpha) = -\frac{\sin(b)}{\sin(\Delta - \delta\Delta)} \quad (17)$$

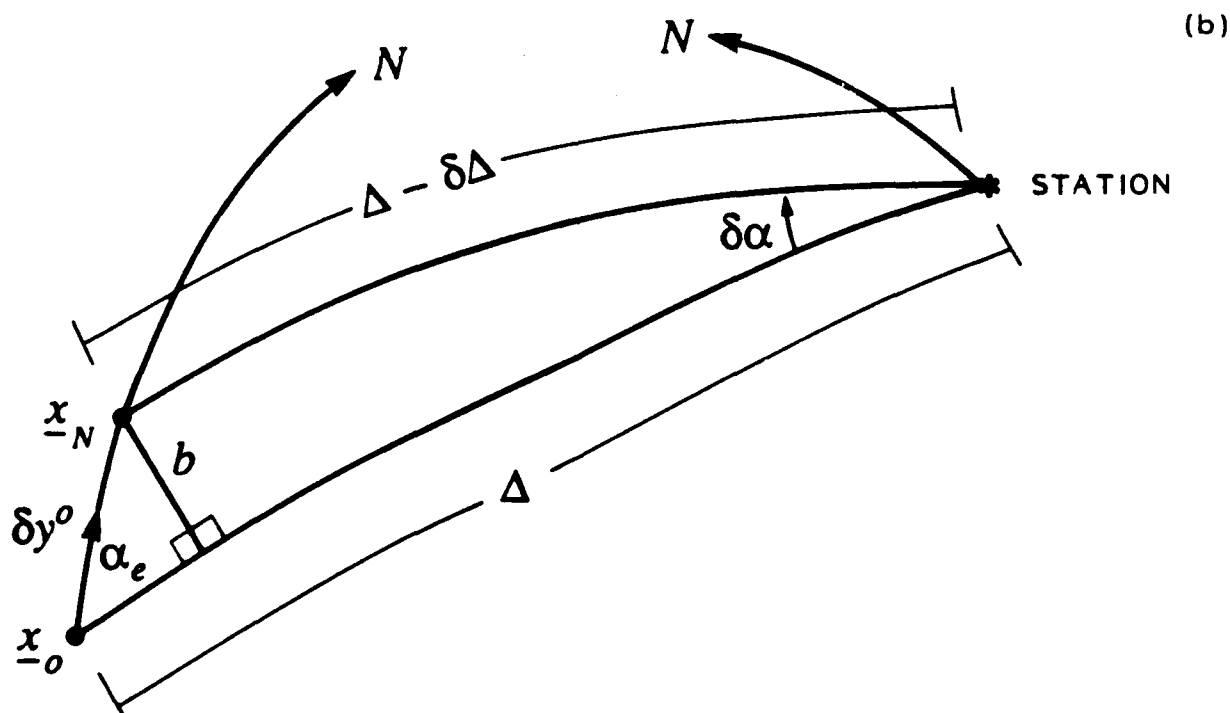
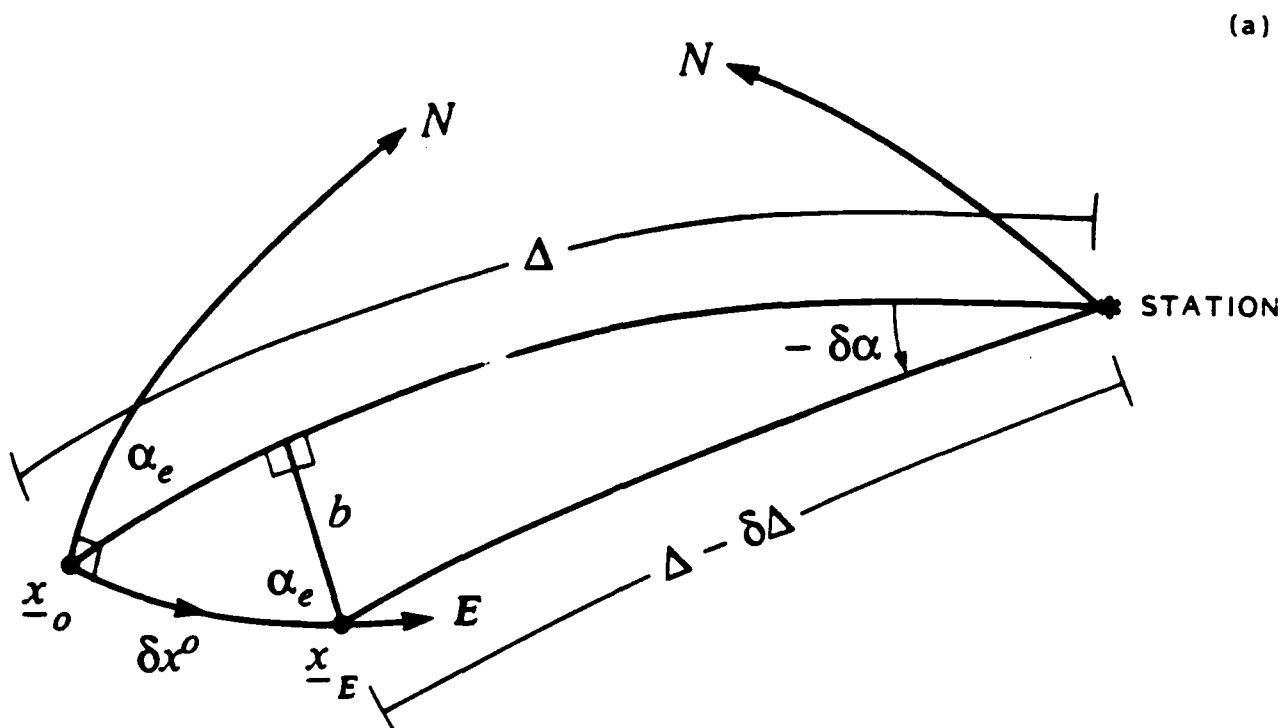


Figure 1. Geometry for determining the partial derivatives of azimuth (α) with respect to cartesian coordinates (a) x (easterly direction) and (b) y (northerly direction).

Assuming angle $\delta\alpha$ and sides b and $\delta\Delta$ are small, we simplify equation (17):

$$\delta\alpha = - \frac{b}{\sin(\Delta)}. \quad (18)$$

The small distances involved permit δx° at the event to be estimated using plane trigonometry:

$$\delta x^\circ = \frac{b}{\cos(\alpha_e)}. \quad (19)$$

Combining (18) and (19) and changing units we obtain:

$$\frac{\partial\alpha}{\partial x} = - \frac{\cos(\alpha_e)}{\sin(\Delta)} \frac{0.0090^\circ}{km}. \quad (20)$$

The partial with respect to y are obtained in a similar fashion (see Figure 1b):

$$\frac{\partial\alpha}{\partial y} = \frac{\sin(\alpha_e)}{\sin(\Delta)} \frac{0.0090^\circ}{km}. \quad (21)$$

The partials of azimuth with respect to depth (z) and origin time (T_o) are zero. The non-linearity of these partials poses little problem, as long as the first trial solution is within the same quadrant as the correct azimuth for most of the stations providing azimuth data. This criterion is easily satisfied by using the azimuth data themselves to compute the first trial location, as explained below.

We have written a program (*TTAZLOC*) implementing this location procedure in the following way. If there are data from multiple arrays, the initial trial location (\underline{x}_c) is defined as the crossing point of great-circle paths along the best determined (smallest standard deviation) azimuths from the two closest arrays. If azimuth data are available from only one array, \underline{x}_c is assumed to be at a range of 100 km and at the best determined azimuth. If no azimuth data are available, \underline{x}_c is placed near the station reporting the earliest arrival time. The theoretical arrival

times and azimuths are calculated from this trial hypocenter, and the data residuals are determined. The \underline{A} matrix is filled by computing finite difference travel-time partials for the appropriate phases, and by using (20) and (21) to compute the azimuth partials. We next normalize \underline{r} and \underline{A} by the appropriate standard deviations (5) and compute the parameter perturbations using (6). The program iterates until convergence criteria are met. The epicentral error ellipse, the depth uncertainty, and the origin time uncertainty are all computed separately, using the method of Jordan and Sverdrup (1981) described in the previous section.

DESCRIPTION OF EXAMPLES

The motivation for developing *TTAZLOC* was the need to compute accurate locations for a sparse network including NORESS-type arrays, and we will illustrate its application with examples from a network including two arrays. In this section we describe these arrays and the examples. The two small-aperture arrays are NORESS, located within NORSAR, and FINESA, located near Helsinki, Finland. NORESS includes a single center element and 24 others distributed in three concentric rings. The diameter of the outer ring is 3 km. Its design and capabilities are described in a number of papers by the NORSAR staff, including Mykkeltveit, *et al.* (1983), Mykkeltveit and Bungum (1984), and Bungum *et al.* 1985. FINESA (Korhonen *et al.* 1986) is composed of a center element, eight elements in two concentric rings (the largest of which has a diameter of about 600 m), and a tenth seismometer located approximately 1 km from the center. The locations are listed in Table 1 and plotted in Figure 2.

Table 1

Center Element Location			
Array	Abbreviation	Latitude	Longitude
NORESS	NOR	60.735 N	11.542 E
FINESA	FIN	61.444 N	26.079 E

The velocity model in Table 2 is used for regional phases recorded at both arrays. This is most appropriate for travel paths to NORESS from the east, and there are known differences for paths from the west and for the vicinity of FINESA (Mykkeltveit, personal communication). However, these differences are small, and we choose to keep the model simple for these examples. Incorporation of laterally and vertically varying velocity structure into the location procedure is straightforward.

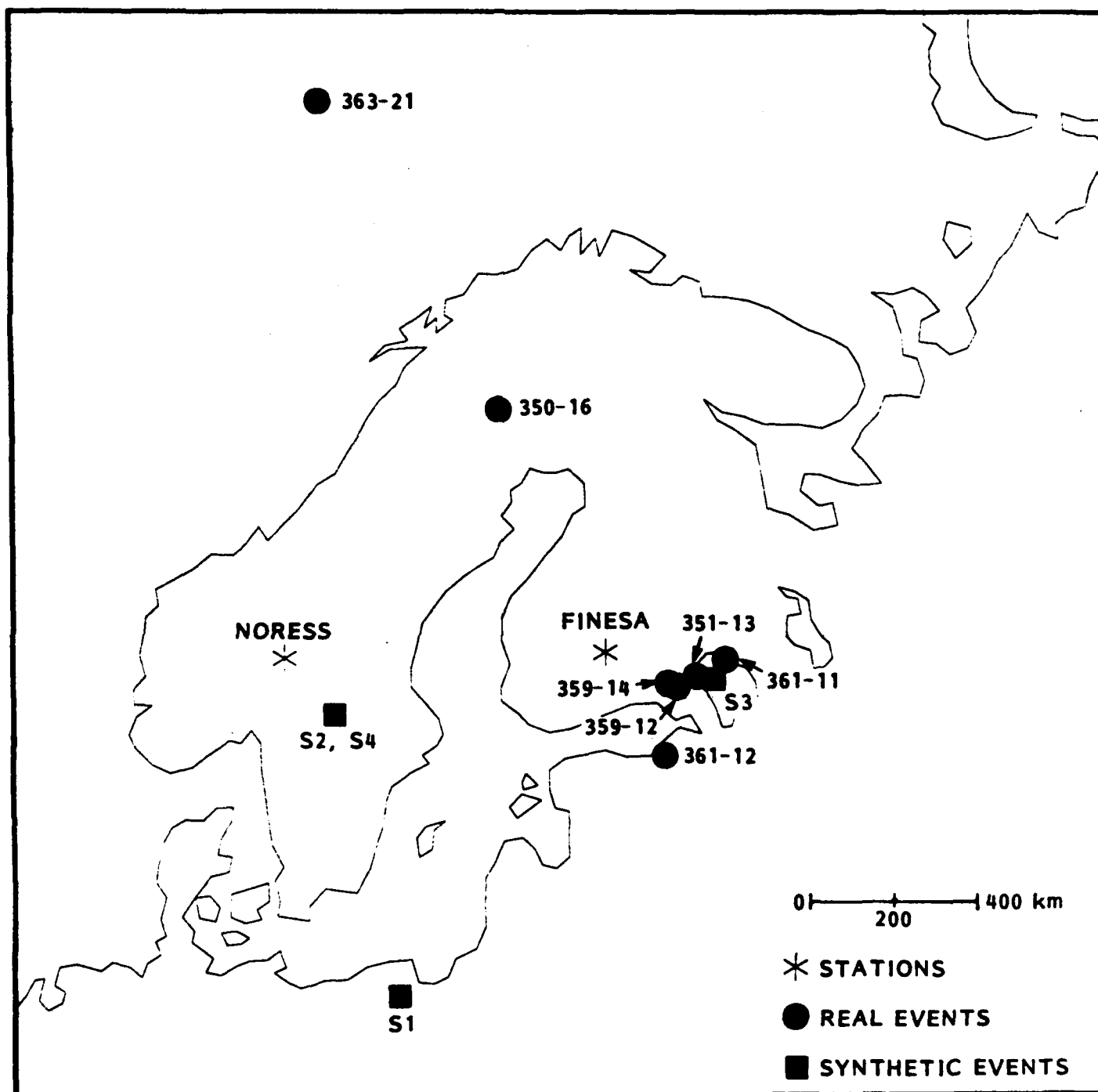


Figure 2. Locations of arrays (asterisks), synthetic events (boxes) and real events (circles) used in this study. See also Table 3.

Table 2

Velocity Structure.				
Layer	Thickness (km)	V_P (km/s)	V_S (km/s)	V_{Lg} (km/s)
1	16	6.2	3.6	3.5
2	24	6.7	3.9	
3	15	8.1	4.7	
4		8.3	4.8	

The examples include actual and synthetic data. The actual data are from seven regional events occurring between December 16 and 29, 1985. Most have been located by independent networks, and these locations are given in Table 3 and plotted in Figure 2. Five of the seven are explosions in known mines and are probably accurate to ± 1 km. Event 359-14 (Julian date 359, hour 14) appears to be a mine blast, but was not detected by the local networks. The location for the seventh event (363-21) is from the Preliminary Determination of Epicenters and may be in error by tens of kilometers. We assume that the focal depths for the mine blasts are zero. The depth for 363-21 is unknown.

We also consider four hypothetical events that allow us to isolate certain features of the solutions, and these appear at the bottom of Table 3. For these examples, synthetic arrival-time and azimuth data are generated by tracing rays through the structure of Table 2.

Table 3

Independent Event Locations					
Designation	Type	Latitude	Longitude	Depth	Magnitude
350-16	Mine Blast	67.1	20.6	0	m_L 2.5
361-11	Mine Blast	61.4	31.6	0	m_L 2.2
359-12	Mine Blast	60.9	29.3	0	m_L 2.1
359-14	Mine Blast*	61.0	28.9	0	m_{LG} 2.6
361-12	Mine Blast	59.4	28.5	0	m_L 2.4
351-13	Mine Blast	61.1	30.2	0	m_L 2.5
363-21	Earthquake	73.2	5.7	?	m_b 4.7
S1	Synthetic	54.0	18.0	0	
S2	Synthetic	60.0	14.0	0	
S3	Synthetic	61.0	31.0	0	
S4	Synthetic	60.0	14.0	20	

* Location from this study. No independent location available.

The location solutions are obtained as part of a larger system for automatically processing data from a network including arrays. As currently implemented, the signal detection is done with relevant portions of the *RONAPP* program (Mykkeltveit and Bungum, 1984). Signal detection occurs when the ratio of short-term average amplitude to long-term average amplitude (STA/LTA) is greater than an empirically-determined threshold on one or more of a set of fixed beams. The beam parameters are slowness, azimuth, band-pass filter, and weighting applied to individual when forming beams. Figure 3 shows two beams for NORESS and FINESA for event 361-11. For each array the top trace is a delay-and-sum beam at high velocity (8 km/s) and high frequency (2 to 8 Hz). It is designed to accentuate P arrivals. The lower trace is an incoherent beam (rectify, delay-and-sum). It is beamed for low velocity (4.5 km/s) and low frequency (2 to 4 Hz), and so is configured to accentuate Lg and Sn arrivals. Both beams are steered toward the actual location of the event. To compute the location, the required information includes the onset time, phase identity (i.e., Pn, Pg, etc.), and azimuth for each detection. The onset time is determined with the *RONAPP* algorithm (Mykkeltveit and Bungum, 1984). Phase identification is a complex task done by a rule-based expert system, but a description of this is outside the scope of this study.

Estimates for the azimuth for each detection are computed with frequency-wavenumber (f-k) analysis. We are using a program developed by Kvaerna and Doornbos (1986), which computes the average power versus wavenumber over a band of frequencies. Examples of power contours computed with this method for the NORESS detections of Figure 3 are shown in Figure 4. The frequency averaging is done over one octave centered about the dominant frequency of the detection. Estimates of the slowness and azimuth of the incoming wave are provided by the wavenumber of the peak of the power contours. For assigning a variance to the azimuth estimate, we need a measure of the quality of the solution. A simple measure is obtained from the relative height of the highest peak. We call this *fkq*. It is assigned the value 1 when the amplitude of the second peak is more than 6 dB less than the highest peak. The assigned *fkq* is 2, 3, and 4 when the difference between the first and second peaks is 4 to 6 dB, 2 to 4 dB, and 0 to 2 dB, respectively. The *fkq* for the spectra in Figures 4a, b, and c are indicated.

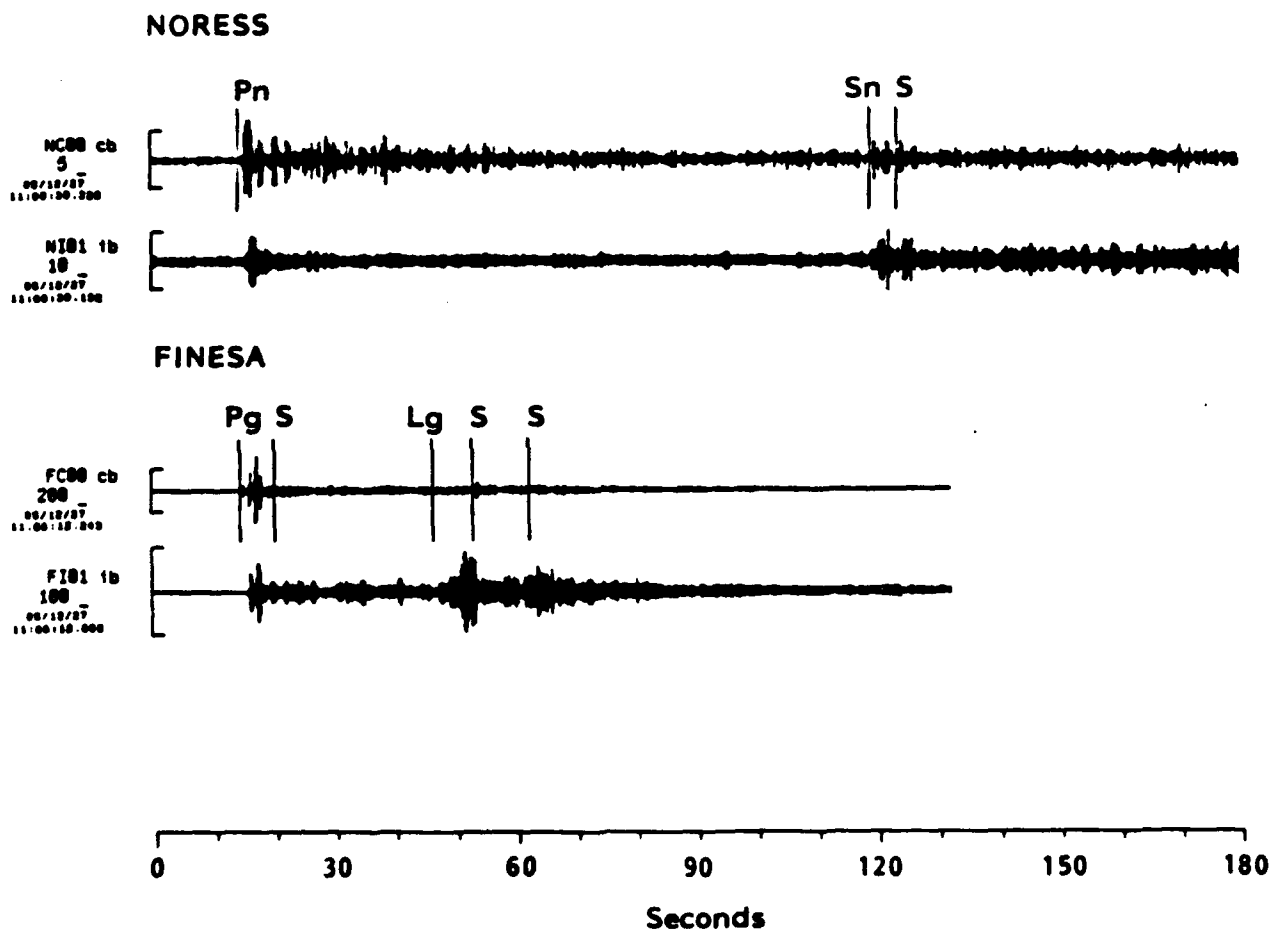


Figure 3. Examples of NORESS (top) and FINESA (bottom) beamed seismograms for event 361-11. The top trace for each array is a coherent, high velocity, high frequency beam. The bottom trace is an incoherent, low velocity, low frequency beam. All beams are steered to the actual event azimuth. See text for details.

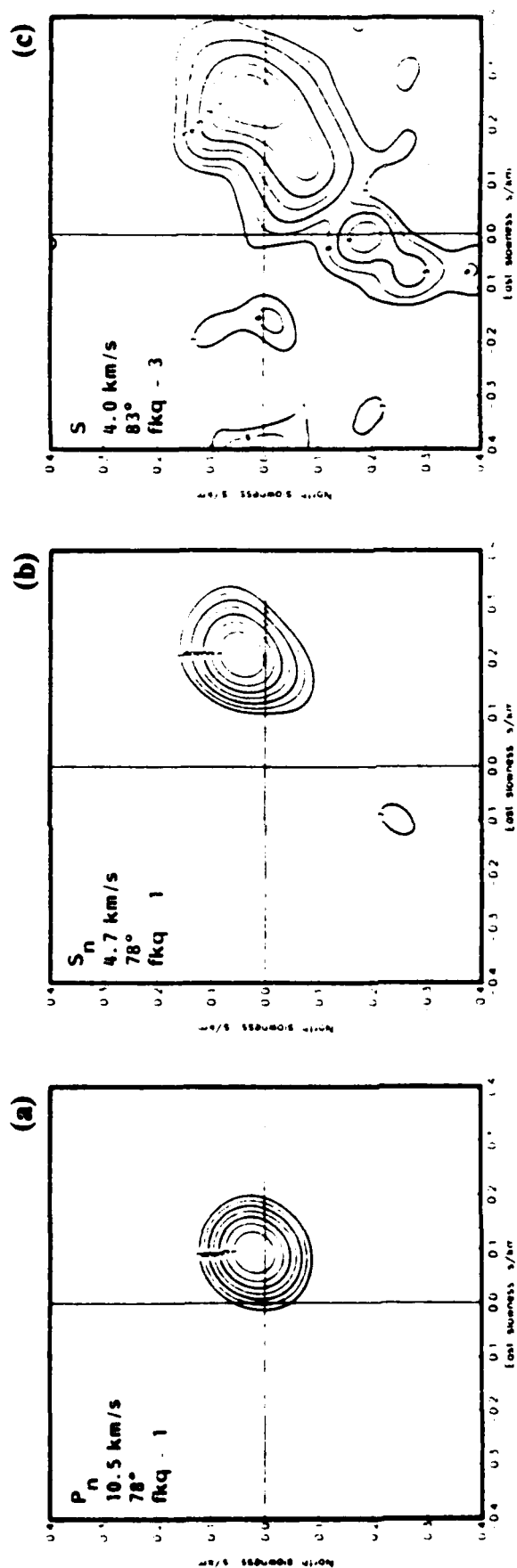


Figure 4. Power contours computed using the broad-band frequency-wave number program of Kvaerna and Doombos (1986). The power is contoured as dB down from the peak value, and is plotted versus north and east slowness.

The location solution and confidence bounds on that solution depend on the variance assigned to the data. Currently, we compute the arrival-time (σ_{LP} and σ_{LS}) and azimuth (σ_α) standard deviations automatically using the formulas described below. With more experience these relations will be refined to more accurately portray the true uncertainty in the hypocenter estimate (as will be illustrated in a later section).

The σ_i represent uncertainties in the arrival time due to random errors in estimating the arrival time and random deviations from the theoretical earth model. They are computed as functions of the STA/LTA (snr) and STA/LTA threshold (bth) for the beam upon which the detection is declared. The σ_i for Pn and Pg phases is given by:

$$\sigma_{LP} = \begin{cases} 0.75 & \text{for } snr > 2 \text{ } bth \\ 2.25 - 0.75 \text{ } bth/snr & \text{for } bth \leq snr \leq 2 \text{ } bth \end{cases} \quad (22)$$

That is, the standard deviation on the arrival time is assumed to be 0.75 seconds, except for small snr , when it is increased to a maximum of 1.5 seconds. Sn and Lg phases are assumed to have double the standard deviation of P-type phases with the same snr/bth ratio. That is, they vary from 1.5 to 3.0 seconds.

The azimuthal standard deviations (σ_α) are based on the beam resolution at the selected frequency and the quality of the particular solution (given by the fkq). The beam resolution is determined from the theoretical beam pattern for the dominant frequency; in particular, from the azimuthal difference between the peak power and the 1 dB contour (daz). The daz and fkq are related to σ_α by:

$$\sigma_\alpha = \begin{cases} 0.5 \text{ } da_z, & \text{for } fkq = 1, \\ 0.75 \text{ } da_z, & \text{for } fkq = 2, \\ da_z, & \text{for } fkq = 3 \end{cases} \quad (23)$$

Detections with $fkq = 4$ are not used for location. Note that σ_α is proportional to daz , which increases with phase velocity and is inversely proportional to frequency. The daz also depends on array geometry, with the smaller and asymmetric FINESA array having larger and

azimuthally-dependent daz for a given frequency. Note that the standard deviations represent random processes and may not adequately account for systematic bias due to, for example, lateral heterogeneity in earth structure. The values computed with (22) and (23) are reasonable, but somewhat arbitrary. The only way to validate them is to study how well the resulting confidence ellipse represents the true precision of the location solutions. The standard deviations assigned to the synthetic data are given in Table 4. These values are slightly larger than those usually encountered with real data, but this choice highlights the effects of adding or subtracting a datum.

Table 4

Standard Deviations for Synthetic Data.		
Data	Symbol	Value
Pn, Pg arrival times	σ_{LP}	1.5 s
Sn, Lg arrival times	σ_{LS}	3.0 s
Pn, Pg, Sn, Lg back azimuths	σ_{α}	10^0

LOCATION SOLUTIONS

In this section, we demonstrate the use of *TTAZLOC* with examples. In particular, we are concerned with an assessment of the precision and accuracy of the solutions obtained. The precision is represented by the size of the hypocentral confidence ellipsoid. This depends on the data residuals, data variances, uncertainty in these variances (the K in equations 12 and 13), and the parameter covariance matrix, which is a function of network geometry. Thus, the validity of the confidence ellipsoid as a measure of precision depends on the validity of both *a priori* and *a posteriori* assumptions about random characteristics of the data. If there is bias in the data, solutions can be precise, but not accurate. The accuracy is simply the proximity of the actual location to the estimated location, and depends largely on the validity of the assumption that the elements of the residual vector \underline{r} are samples of zero-mean, random processes. Systematic errors or bias due to structural heterogeneity, station elevation, etc., reduce the accuracy. Data selection and weighting also play a role in determining location accuracy.

We illustrate the capabilities of *TTAZLOC* by examining solutions for the hypothetical and real events of Table 3 and Figure 2. Synthetic data furnishes a level of consistency that allows solutions for different events and for different subsets of data from a given event to be easily compared. We use these solutions to demonstrate the effect on location precision of varying the number, type, and quality of data used. We also present some examples where arrival times are not adequate to determine a solution, so the azimuths are critical.

Application of *TTAZLOC* to data from actual events demonstrates the use of our technique in practice. We show how the *a priori* variance scale factor s_K^2 and associated uncertainty (represented by K) are derived from preliminary solutions for these events. We then use these quantities to determine new "K-weighted" confidence bounds on the solutions. Comparing our solutions to well-constrained independent locations, we assess the accuracy of locations with and without azimuth data and the validity of the s_K^2 , K , σ , and the K-weighted confidence ellipsoids.

Application to Synthetic Data

Without azimuth information, the determination of event location and confidence bounds with data from a single array is impossible. Figures 5 and 6 show single-array locations and confidence ellipses computed by *TTAZLOC* from hypothetical NORESS detections of signals from synthetic events. The base map shows the region around the NORESS and FINESA arrays, which are indicated by asterisks. The interstation distance is about 780 km. Dashed lines radiating from an array show the azimuth of incoming phases. Each such line is labeled at its termination by a phase identifier. Two character identifiers (PN, PG, SN, LG) are phases used to locate the event, while single character markers denote other detected phases from the same event. Sparsely-dotted arcs are drawn to azimuths that are $\pm 2\sigma_\alpha$ from the mean azimuth estimate. The 90% confidence ellipses are shown for each location solution. The depths are fixed at zero unless stated otherwise. All our solution plots are in this format. For the synthetic examples we set $s_K^2 = 1.0$ and $K = \infty$ (see equations 12 and 13). The resulting confidence ellipsoids are χ^2 error bounds, and thus they are independent of the data residuals. They depend only on the parameter covariance matrix, which reflects the geometry of the observing network and the assigned data variances.

The single-array solutions depend on the assigned data variances in a simple way. The radial dimension of the epicentral error ellipse is controlled by the arrival-time variances, and the azimuthal dimension is controlled by both the azimuthal variances and the distance to the event. These relationships are illustrated in Figure 5 (Table 5). The effect of event distance on the confidence ellipse is demonstrated by comparing ellipses (1) and (2). The two solutions differ only in the Pn - Sn time separation of the data used. This illustrates what is apparent from the geometry and (20) and (21); the location constraint imposed by azimuth data decreases inversely with distance Δ . Ellipses (2) and (3) differ only in the standard deviation assigned to the azimuth measurements. Decreasing σ_α from 10° to 3° produces a proportionate decrease in the azimuthal dimension of the χ^2 confidence region.

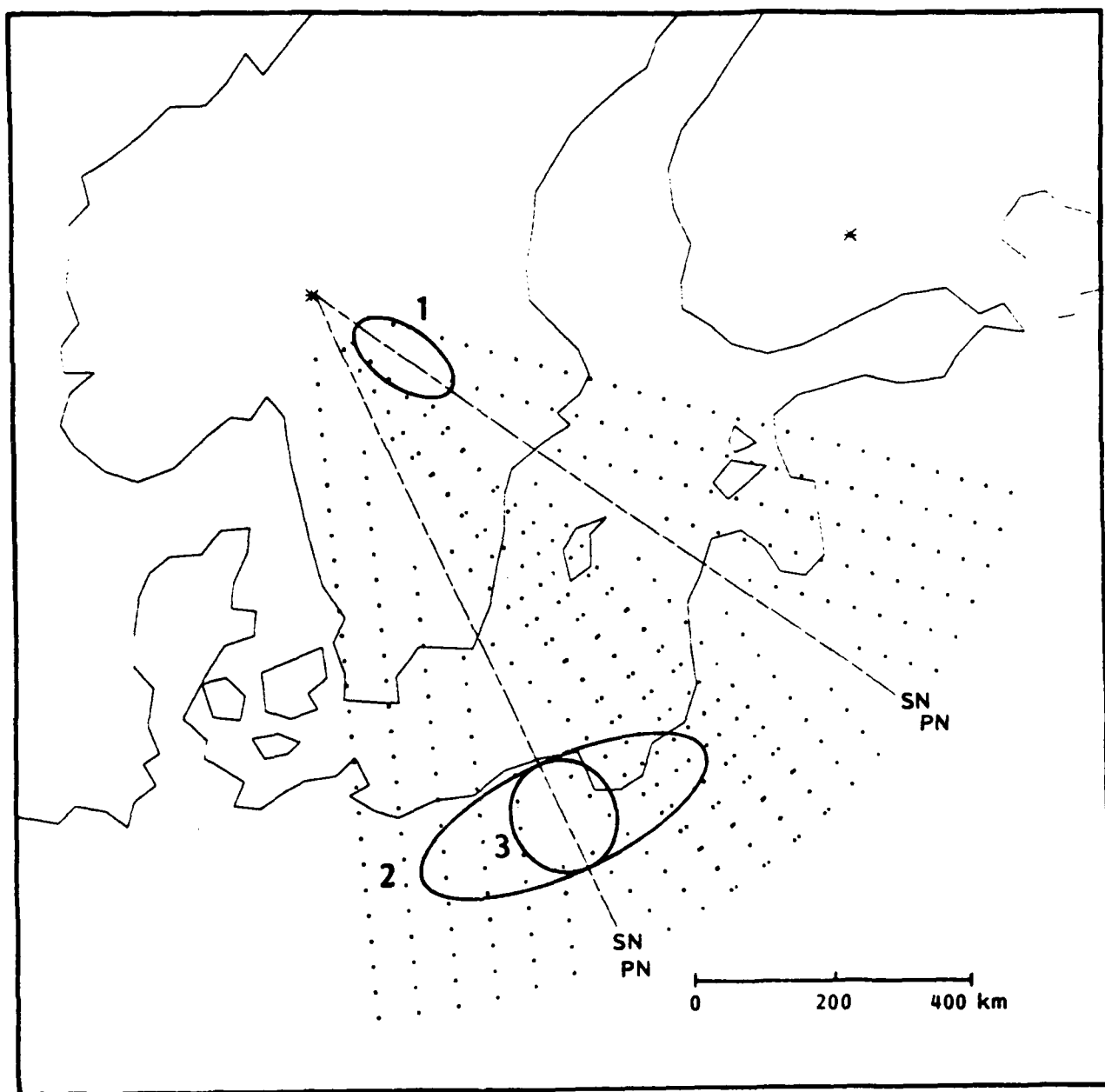


Figure 5. Confidence ellipses (90%) computed using Pn and Sn data from synthetic events recorded at NORESS. NORESS and FINESA arrays are plotted as asterisks. Azimuths of arrivals are shown by dashed lines. The $\pm 2 \sigma$ error on azimuth measurements are indicated by the dotted arcs. The examples are: (1) event S2 at 1.4° distance; (2) S1 at 7.6° ; and (3) S1 with azimuth standard deviation reduced from 10° to 3° .

Table 5

Azimuthal Constraint as Function of Event Distance and Data Uncertainty. Location Solutions of Figure 5.							
	Event Distance	σ_α	Event	Latitude	Longitude	Semi-major axis (km)	Semi-minor axis (km)
(1)	1.4 ⁰	10 ⁰	S2	60 ⁰	14 ⁰	81	42
(2)	7.6 ⁰	10 ⁰	S1	54 ⁰	18 ⁰	223	81
(3)	7.6 ⁰	3 ⁰	S1	54 ⁰	18 ⁰	81	74

The χ^2 ellipses become more precise (i.e., smaller confidence ellipsoid) as more data are used for the solution. This is illustrated in Figure 6 (Table 6). Ellipse (1) is for a location with arrival-time data for Pn and both arrival time and azimuth data for Sn. This is the minimum data set for a unique solution for latitude, longitude and origin time. If we add the Pn azimuth, ellipse (2) is the result. Thus, a second azimuth datum with the same standard deviation reduces the azimuthal uncertainty about 30%. Ellipse (3) is the single array solution for all arrival time and azimuth information for Pn, Sn and Lg. The solution precision could be made still better with azimuths from additional detections (e.g., P coda detections). However, further study is required to be sure that adding such secondary detection data will generally act to improve location accuracy, as well as the precision measured by the confidence ellipsoid.

Table 6

Effects of Additional Data Location Solutions of Figure 6.						
	Notes	Event	Latitude	Longitude	Semi-major axis (km)	Semi-minor axis (km)
(1)	Pn (t), Sn (t, α)	S1	54 ⁰	18 ⁰	315	81
(2)	Pn, Sn (t, α)	S1	54 ⁰	18 ⁰	223	81
(3)	Pn, Sn, Lg (t, α)	S1	54 ⁰	18 ⁰	182	41

Azimuth data can play a major role in location solutions determined by a network of stations, especially when the detecting network is small and/or the event is close to at least one station. For instance, for small events it is common for the arrays to detect only a single phase. In this

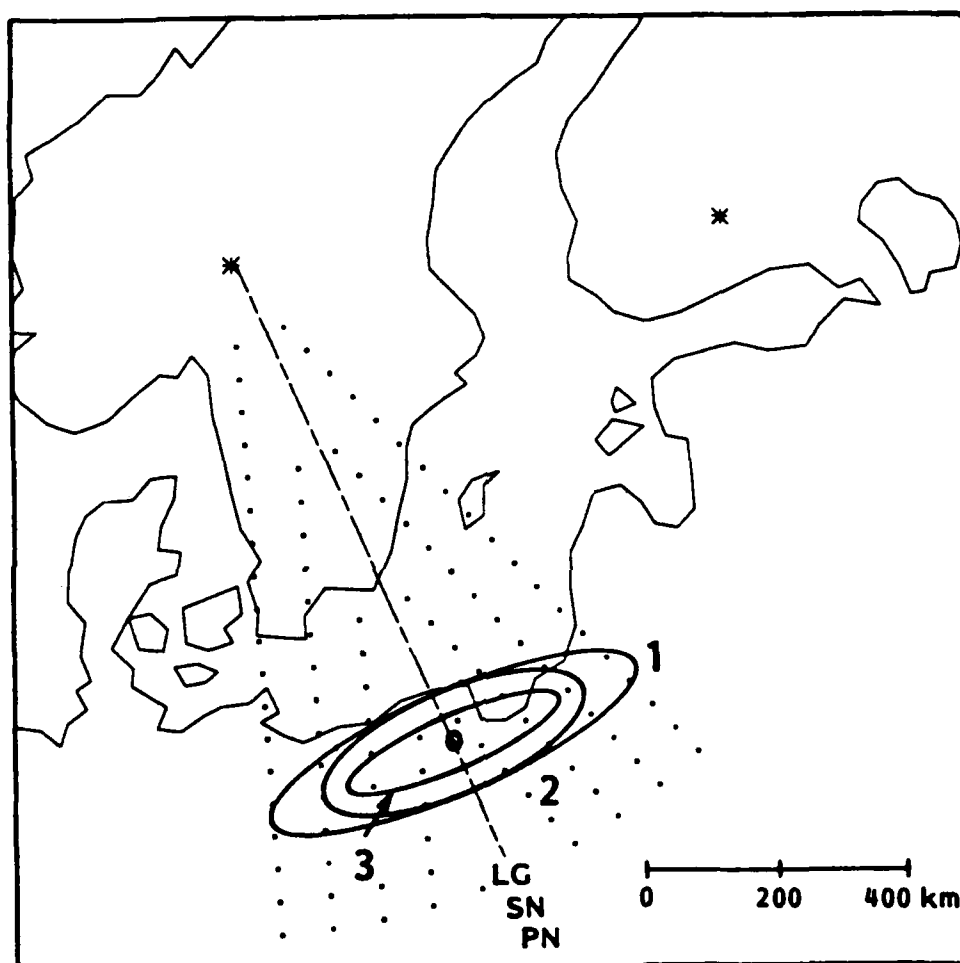


Figure 6. Effect of additional data on the shape of the single-array confidence ellipses. The data included are: (1) Pn arrival time and Sn time and azimuth; (2) Pn and Sn times and azimuths; (3) Pn, Sn and Lg times and azimuths. (Table 6).

situation no single-array location is possible. If two arrays each detect a single phase, a location is not possible with arrival times alone. However, with azimuth data one can compute a unique location and its confidence ellipse, as illustrated in Figure 7 and (Table 7). Latitude and longitude (but not origin time) can be estimated with the azimuths alone.

Table 7

Event Located with a Single Phase at Each Array. NORESS - Sn, FINESA Pn (Figure 7).						
	Distances NOR/FIN	Event	Latitude	Longitude	Semi-major axis (km)	Semi-minor axis (km)
(1)	1.4/6.1 ⁰	S2	60 ⁰	14 ⁰	60	20

In Figure 8 (Table 8) we compare solutions with arrival time only (using azimuth estimates only to select the appropriate quadrant) with solutions obtained with azimuths formally included in the inversion. For the farther event, solutions with and without azimuth data are indistinguishable. This is not unexpected in view of the fact that azimuthal constraint decreases with distance (Figure 5), and that for this example the arrival times from the two arrays provide near-orthogonal constraints on the solution. For the closer event the NORESS azimuths provide a strong constraint, and they reduce the northerly dimension of the confidence ellipse to less than half that computed with arrival times alone.

Table 8

Effect of Including Azimuth in Two-Array Locations Pn and Sn Data (Figure 8).							
	Notes	Distances NOR/FIN	Event	Latitude	Longitude	Semi-major axis (km)	Semi-minor axis (km)
(1)	<i>t</i> only	7.6/8.6 ⁰	S1	54 ⁰	18 ⁰	63	33
(2)	<i>t</i> , α	7.6/8.6 ⁰	S1	54 ⁰	18 ⁰	63	32
(3)	<i>t</i> only	1.4/6.1 ⁰	S2	60 ⁰	14 ⁰	119	14
(4)	<i>t</i> , α	1.4/6.1 ⁰	S2	60 ⁰	14 ⁰	42	14

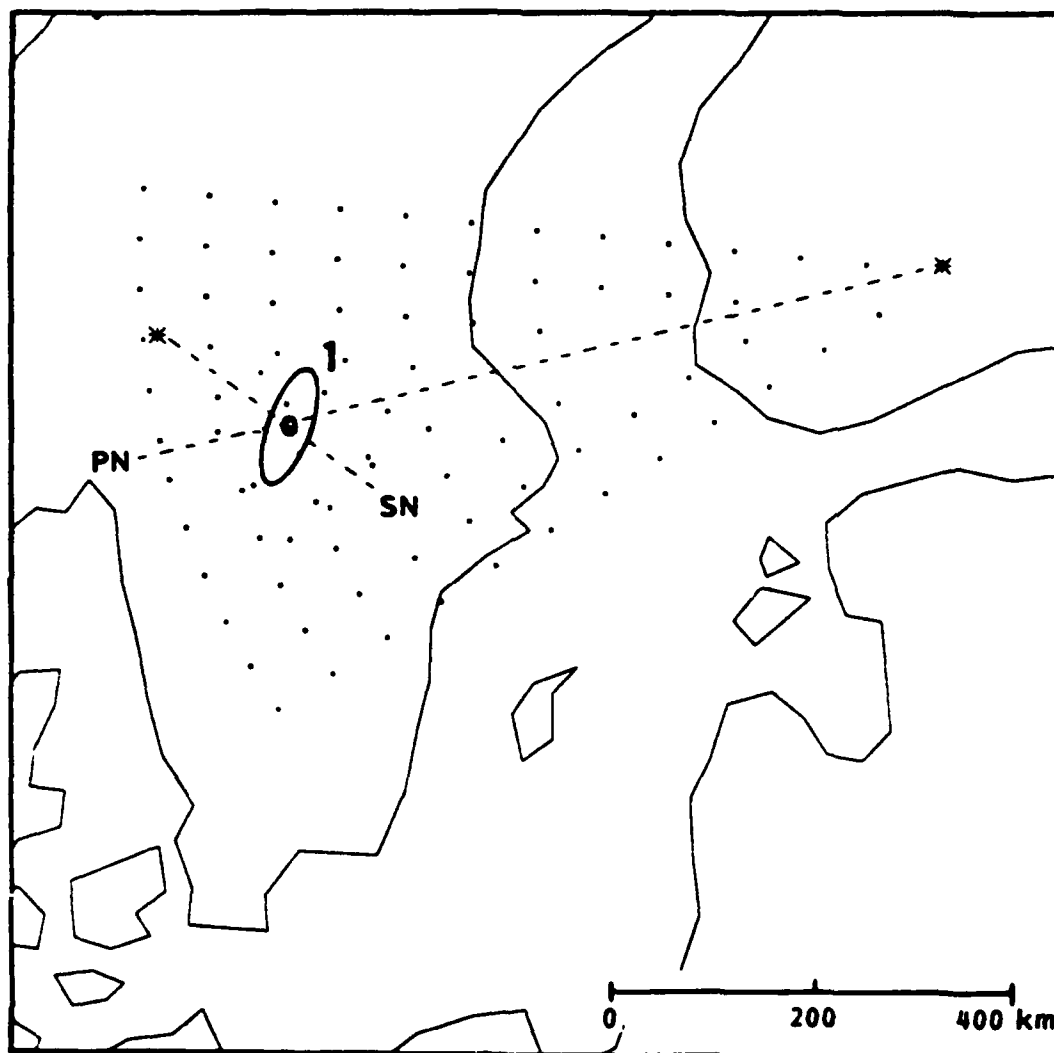


Figure 7. Confidence ellipse for epicenter S2 using only the arrival times and azimuths from a Sn detection at NORESS and a Pn detection at FINESA. (Table 7).

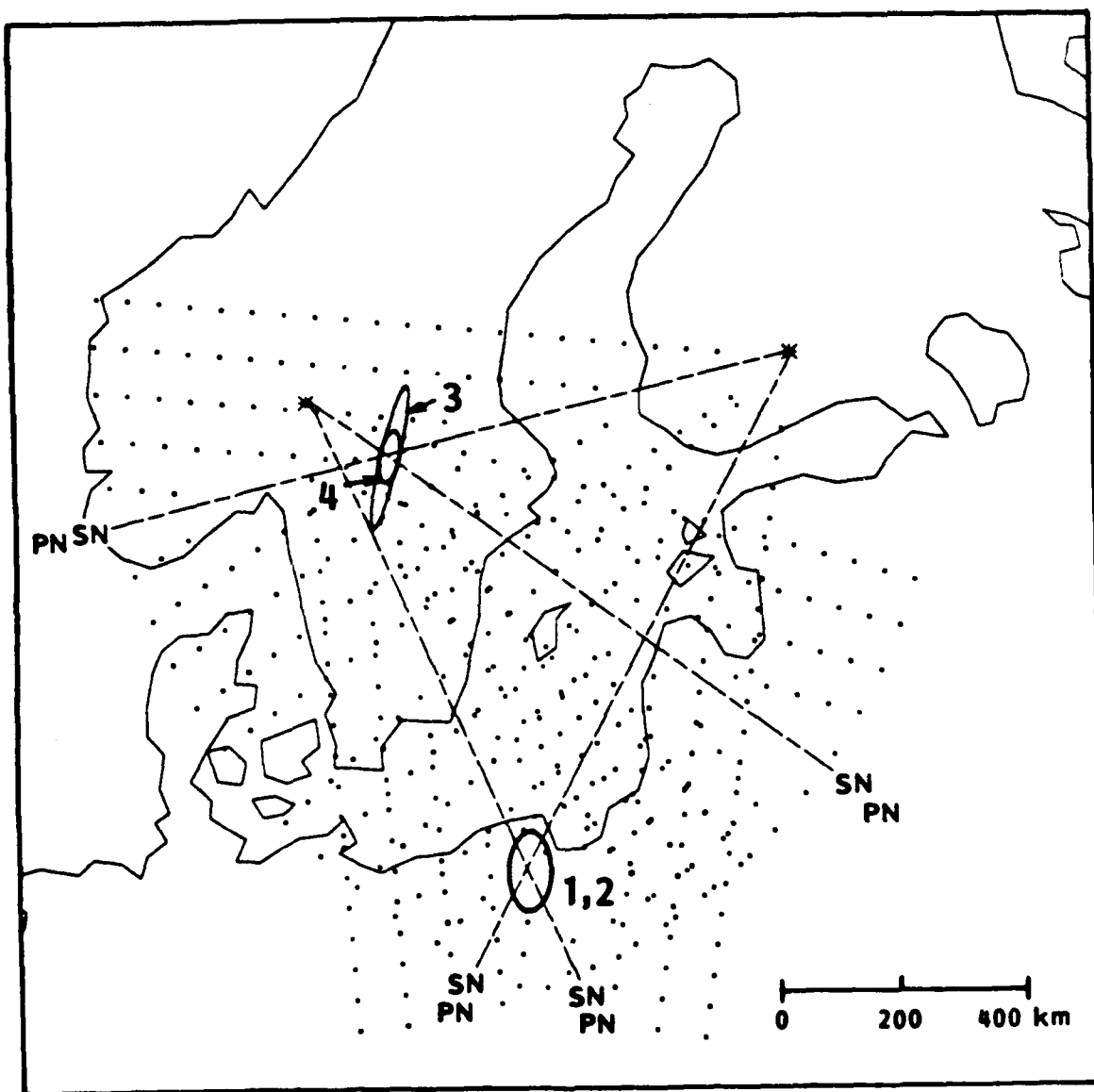


Figure 8. Effect of including azimuth data in two-array location solutions as a function of event distance. All solutions use Pn and Sn data. The ellipses are: (1) epicenter S1 (7.6° from NORESS, 8.6° from FINESA) arrival times only; (2) S1, times and azimuths; (3) epicenter S2 (1.4° from NORESS, 6.1° from FINESA), times only; (4) S2 times and azimuths. (Table 8).

The importance of the azimuth data also depend on the geometry of the problem, and in some geometries azimuth data play a crucial role in defining the precision of the solutions. The most striking example is for an event nearly colinear with two arrays (Figure 9 and Table 9). Without azimuth data, there is little control on the location in the direction perpendicular to the line connecting the arrays. Addition of azimuth information, particularly from the closer array, decreases the dimension of the confidence ellipse in this direction by 75%. In general, we find that when only two NORESS-quality arrays furnish data, the azimuth information provide a significant constraint for events within about 500 km of one array. Azimuth data of lower quality (e.g., from polarization analysis of three-component data) or from more distant events do less to improve location precision.

Table 9

Effect of Azimuth Data for Events Nearly Colinear with Two Arrays. Pn and Sn (Figure 9).							
	Notes	Distances NOR/FIN	Event	Latitude	Longitude	Semi-major axis (km)	Semi-minor axis (km)
(1)	t only	9.4/2.4 ⁰	S3	61 ⁰	31 ⁰	275	57
(2)	t, α	9.4/2.4 ⁰	S3	61 ⁰	31 ⁰	67	57

As we have demonstrated, the importance of azimuth data to constraining location depends on the event distance and the assigned uncertainty. Therefore, the relatively accurate azimuth estimates from NORESS-type arrays are much more important than larger variance azimuths obtained otherwise (e.g., from polarization analysis of three-component data). In general, we find that when only two NORESS-type arrays furnish data, the azimuth information provide a significant constraint for events within about 500 km of an array.

In the final example of this section we briefly examine the depth resolution of our location procedure with data from two arrays. Figure 10 (Table 10) shows recomputed locations for event S4, which has the same epicenter as S2 but a depth of 20 km. The depth was left unconstrained during the location procedure. Ellipse (1) was computed with arrival times and azimuths for three detections, and the resulting depth uncertainty is ± 148 km. Adding a fourth

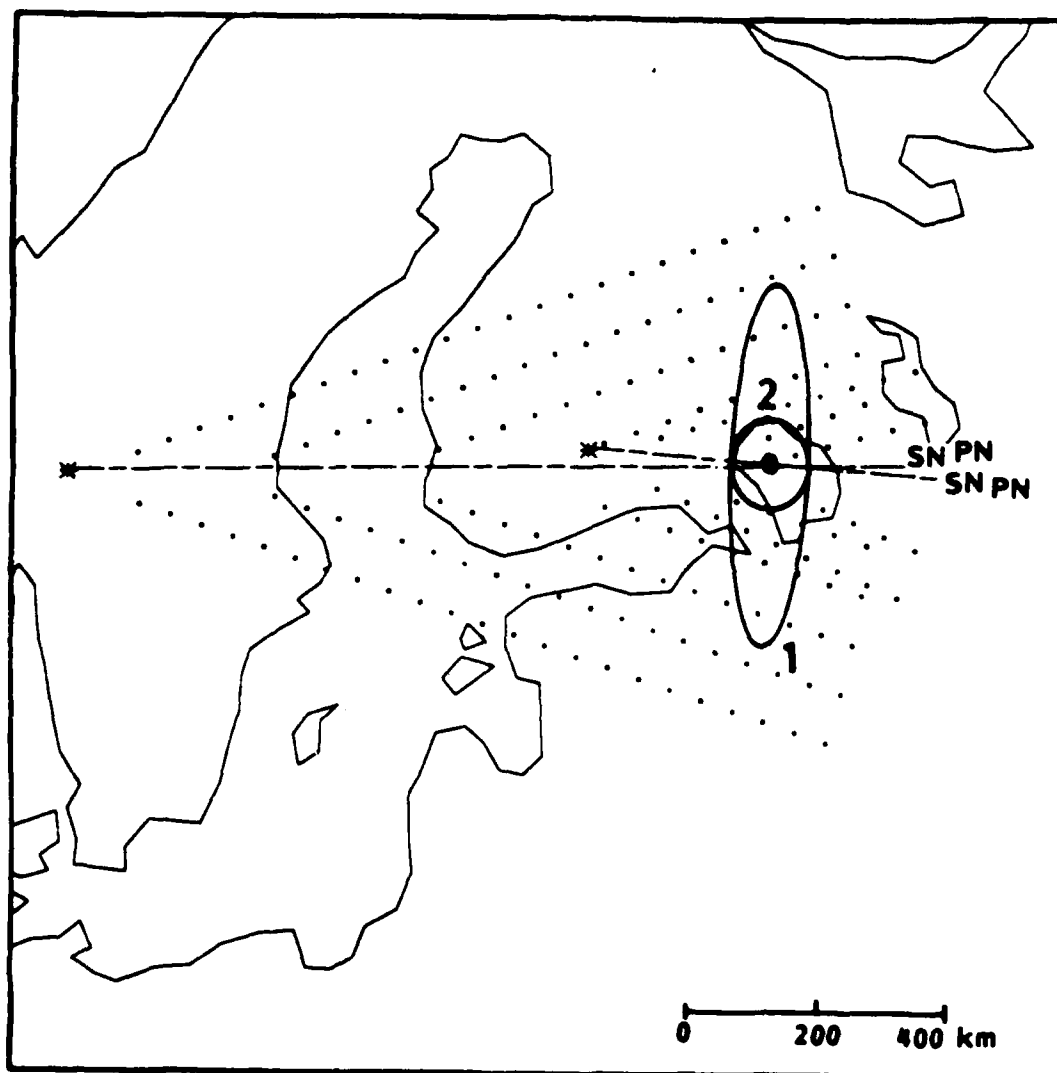


Figure 9. Effect of including azimuth data for an event (S3) almost colinear with NORESS and FINESA. Pn and Sn data are used for both solutions. The ellipses are: (1) arrival times only; (2) times and azimuth. (Table 9).

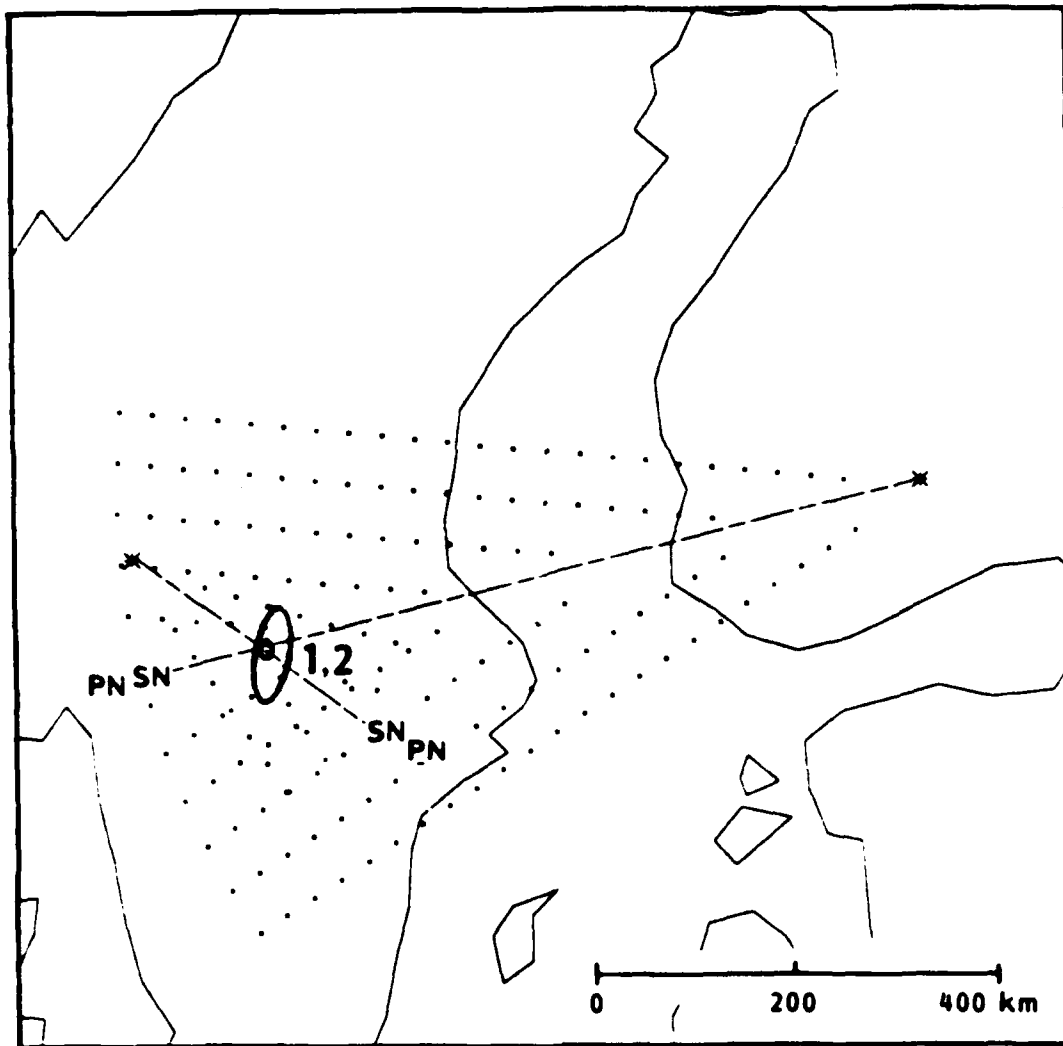


Figure 10. Plan view of confidence ellipsoid for epicenter S4 (20 km depth) with depth unconstrained in the solution. The ellipses are: (1) Pn and Sn arrival times and azimuths at NORESS, Pn time and azimuth at FINESA; (2) Pn and Sn times and azimuths at both arrays.

arrival time and azimuth (Sn from FINESA) has little effect on the epicenter confidence, but the depth uncertainty is reduced by 35% (ellipse 2). While the depths are poorly constrained by either data set, the results suggest that two arrays can give location solutions that at least allow many sub-crustal earthquakes to be identified.

Table 10

Locations with Depth Unconstrained. Pn and Sn Azimuth and Arrival Time (Figure 10).								
	Notes	Event	Latitude	Longitude	Depth (km)	Semi-major axis (km)	Semi-minor axis (km)	Depth Error
(1)	no FIN SN	S4	60°	14°	20	47	17	148
(2)		S4	60°	14°	20	46	15	97

Application to Actual Data

Many of the events recorded by the NORESS and FINESA arrays were located by independent networks operated by Bergen and Helsinki Universities. These local network locations are generally thought to be accurate within 5 -10 km, particularly when the events occur inside the network. Further, many of the recorded events were chemical explosions in known mines, and these are often identified and then located very accurately (within ± 1 km). These independent locations can be used to assess the accuracy of our locations with one or two arrays. In this study we use the seven events of Figure 2 (Table 3) to make a preliminary assessment. We also consider the accuracy of two-array location solutions computed with and without azimuth data. Using a subset of the events, we show how information about the data variances and associated uncertainties (specifically, s_K and K) can be improved with empirical experience, and then incorporated into estimates of location confidence bounds ("K-weighted" ellipses). Comparison of the independent locations to both the traditional F-statistic and K-weighted confidence ellipses demonstrates the utility of the latter approach when the available dataset is small.

For each example we show two tables and two figures. The tables marked "a" give the data and standard deviations used for each location. The "b" tables give the location results including confidence ellipse parameters. In the figures we show the NORESS and FINESA single-array solutions (labeled ellipses 1 and 2), the joint solutions using the time data alone (ellipse 3), and the solution using both time and azimuth data (ellipse 4). The "a" figures show these ellipses computed via the traditional F-statistic approach (equations 7 through 10), while the "b" figures show the corresponding K-weighted ellipses. All solutions presented were computed with the depth constrained to the surface. Note that the location solutions are based on a single velocity model which is most appropriate for paths to the east of NORESS where five of the seven events were located. A somewhat different model is better for the FINESA data and other paths to NORESS, and this has some effect on our examples. Also, the 10-element FINESA array provides less accurate data on detections than the 25-elements of NORESS.

We first consider the accuracy of our solutions by computing the mislocation, ΔL , defined as the difference in kilometers between the *ITAZLOC* and independent epicenters. The first

example, event 350-16, is presented in Figure 11 and Table 11. The independent location (star) is in a mine at 67.1° N and 20.6° E. The available data include Pn arrival time and azimuth at NORESS and arrival time and azimuth for Pn and Sn phases at FINESA. Also detected was a later P phase at NORESS, but we are not now using such secondary arrivals in the location solution. Only FINESA has adequate data for a single array location, but the azimuth estimates are biased to the east, so the solution is not very accurate. The ΔL of the FINESA location is 188 km. For solution (3) we use only the arrival time data from the two arrays, and the ΔL is reduced to 37 km. Because of the inaccuracy of the FINESA azimuth estimates, adding all three azimuth data (solution 4) increases ΔL by 38%.

Table 11a

Data for Event 350-16, 1985.					
Array	Datum	t (min:sec)	σ_t (sec)	α	σ_α
NOR	Pn	46:30.0	0.8	26°	7°
NOR	P	47:54.4		8°	7°
FIN	Pn	46:11.4	0.8	358°	11°
FIN	Sn	47:20.8	2.7	351°	12°

Table 11b

Locations for Event 350-16, 1985 (Figure 11).											
	# Data				Latitude	Longitude	s_s^2	Semi-major axis (km)	Semi-minor axis (km)	ΔL (km)	
	Noress		Finess								
	t	α	t	α							
								F / K	F / K		
				Independent		67.1°	20.6°				
(2)			2	2		67.82°	24.59°	0.19	429 / 343	139 / 111	188
(3)	1			2		67.43°	20.72°	1.00	∞ / 142	∞ / 32	37
(4)	1	1		2	2	67.55°	20.80°	1.02	122 / 121	28 / 28	51

Event 361-11 (Table/Figure 12) is an explosion in a mine about 290 km east of FINESS. The beamformed seismograms for this event were displayed in Figure 3. Both single array epicentral estimates are within 41 km of the true location. The two-array solution computed from only the arrival times (solution 3) is 79 km north of the independent epicenter; twice as far

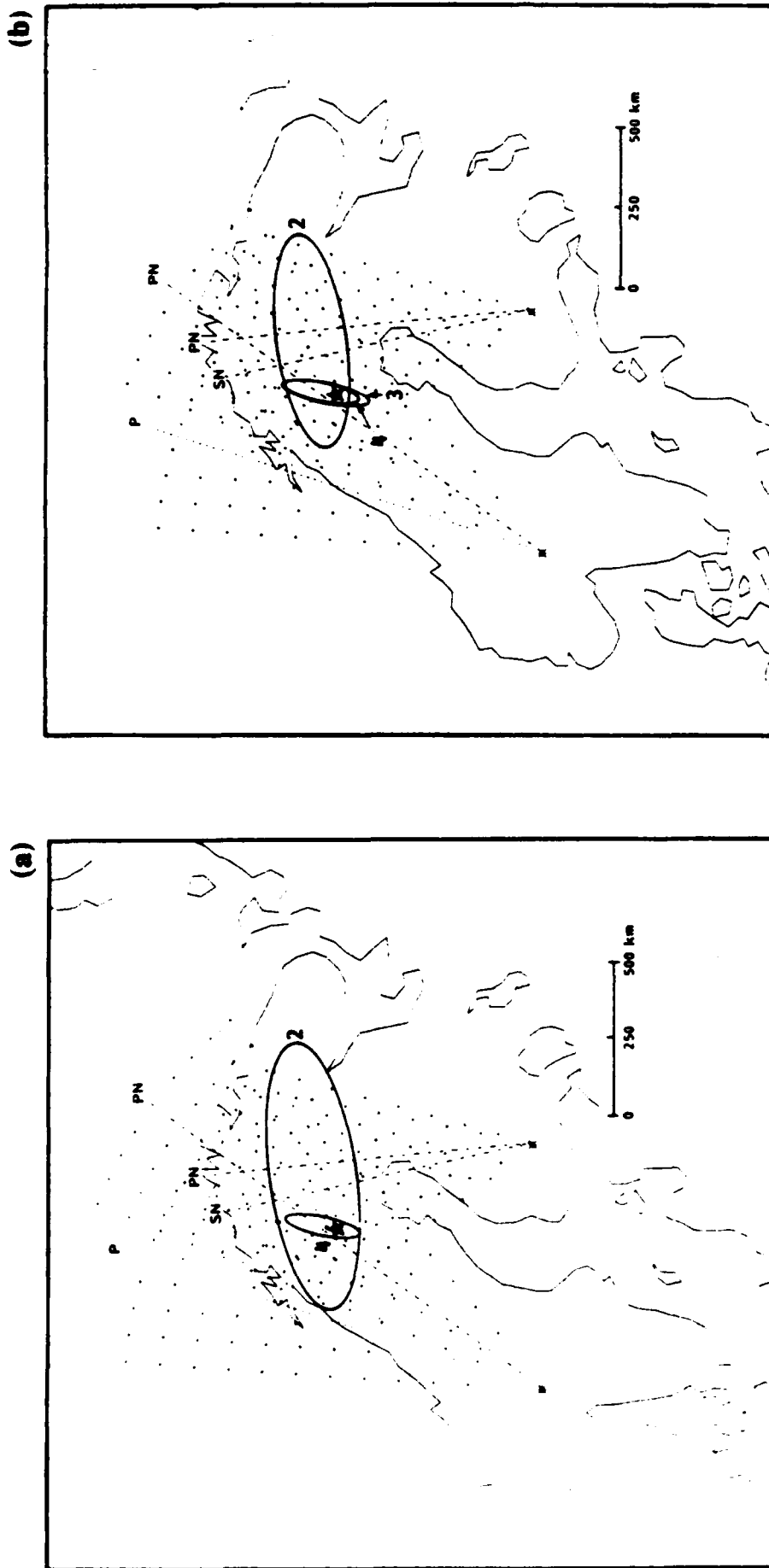


Figure 11. Location solutions for event 350-16. The following format is used for this and subsequent figures. Independent locations are marked by a "star". Confidence ellipses were formed using different subsets of the data and are labeled as follows: (1) NORESS arrival times and azimuths; (2) FINESA arrival times and azimuths; (3) NORESS and FINESA arrival times; (4) NORESS and FINESA arrival times and azimuths. Solutions using all four subsets are not always available. Panel (a) shows the F-statistic confidence bounds. Correspondingly numbered tables give more details. Panel (b) shows the K-weighted bounds with $K = 8$ and $s_K^2 = 2.4$.

away as either of the one-array solutions. This is not surprising given the result of Figure 9 which demonstrates the poor constraint afforded by arrival times at two stations for a nearly colinear event. Adding the corresponding azimuth data, however, improves the location accuracy by about 50%.

Table 12a

Data for Event 361-11, 1985.					
Array	Datum	t (min:sec)	σ_t (sec)	α	σ_α
NOR	Pn	8:44.8	0.8	78°	11°
NOR	Sn	10:29.4	2.8	78°	6°
NOR	S	10:33.8		83°	9°
FIN	Pg	7:14.6	0.8	98°	16°
FIN	S	7:20.5		94°	12°
FIN	Lg	7:46.6	1.5	71°	16°
FIN	S	7:53.3		74°	16°

Table 12b

Locations for Event 361-11, 1985 (Figure 12).							
# Data		Latitude	Longitude	s_s^2	Semi-major axis (km)	Semi-minor axis (km)	ΔL (km)
Noress t	Finess α						
Independent		61.4°	31.6°				
(1)	2 2	61.26°	32.15°	0.00	0 / 327	0 / 111	33
(2)		61.58°	30.92°	1.46	603 / 180	163 / 49	41
(3)	2 2	62.07°	31.10°	5.20	890 / 154	220 / 38	79
(4)	2 2	61.71°	31.30°	1.54	135 / 131	34 / 33	38

Presented in Tables 13 - 17 are the solutions for the remaining five examples. The effect on event mislocation of adding azimuth data based on all seven examples can be summarized as follows. The addition of azimuth data moved the solution farther (relative to the solution using time data alone) from the independent location for one event (350-16). It moved the solution closer for two events (361-11, 351-13) and made no significant difference for two others (361-

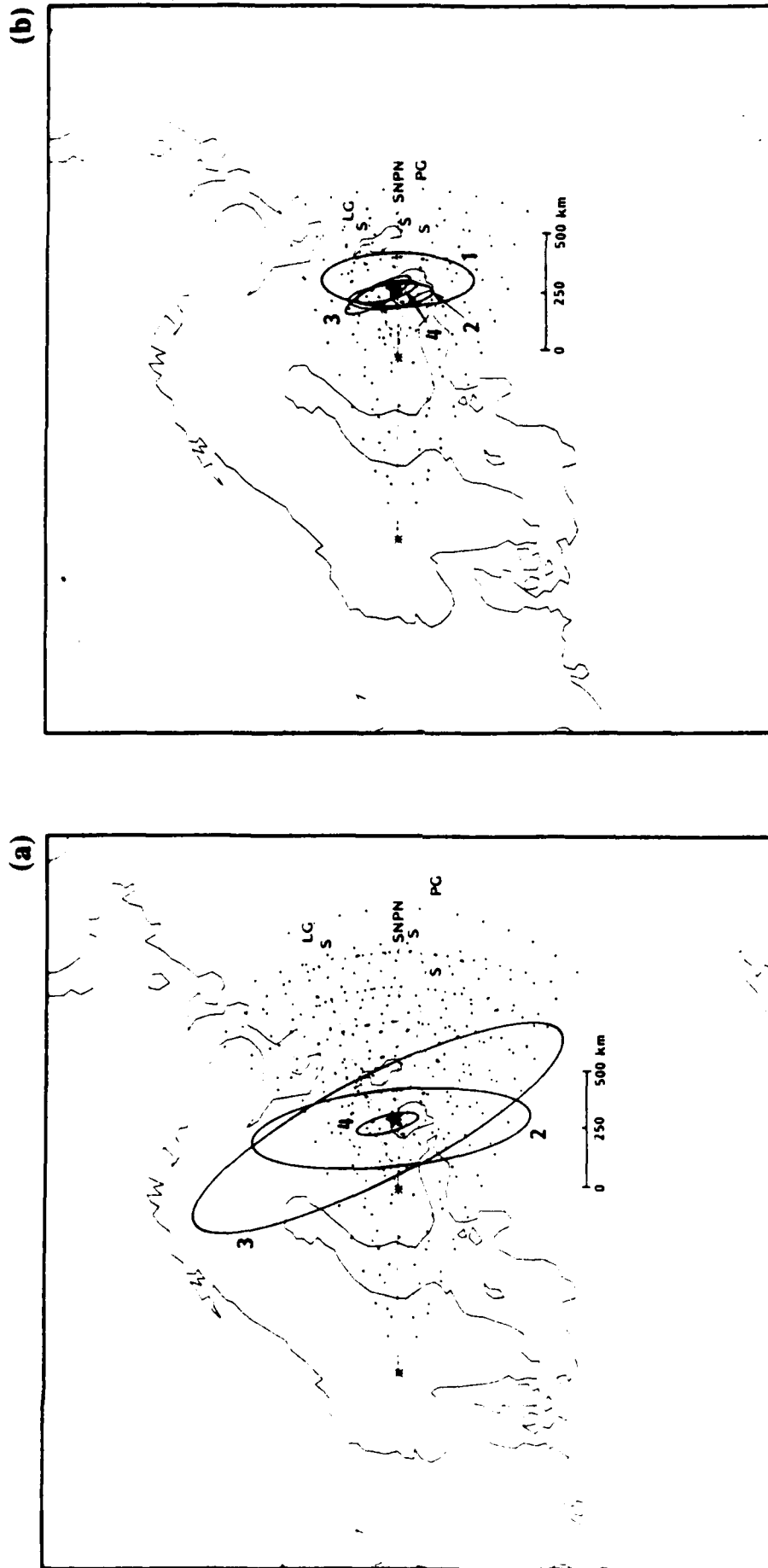


Figure 12. Solutions for event 361-11. (a) F-statistic confidence ellipses, (b) K-weighted confidence ellipses. (Tables 12a and b).

12, 363-21). For two events (359-12, 359-14), *TTAZLOC* failed to converge on a solution using arrival time data alone (arrival time solutions listed in Tables 13 and 14b are the minimum residual solution from the first 20 iterations of each run). However, the program quickly converged on solutions for both events when time and azimuth data were included. These few examples indicate that the azimuth data from these arrays allow computation of reasonable location solutions when they would otherwise be impossible. They also improve location accuracy in many cases.

The estimated precision of these locations is reflected in the 90% confidence ellipsoid computed by *TTAZLOC*. As discussed previously, the traditional F-statistic ellipse is largely controlled by the *a posteriori* estimate of the variance scale factor s^2 . The Jordan and Sverdrup (1981) "K-weighted" ellipse incorporates both *a priori* and *a posteriori* information on the quality of the data, and this permits reasonable confidence bounds even for small data sets. Our examples illustrate the drawbacks of the F-statistic approach when few data are available, and the benefits of incorporating the K-weighting approach.

The dimensions of the F-statistic confidence ellipses for the seven NORESS-FINESA events are given in the column marked "F" in Tables 11 through 17b and plotted in Figures 11 through 17a. As is evident from equations (7) - (10), the uncertainty bounds are a strong function of the normalized sample variance s_s^2 , which in turn depends on the normalized data residual vector \underline{r}_w^2 , divided by the difference between the number of data (N) and parameters (M - 3).

When the available data are highly consistent (relative to the assigned σ), the F-statistic ellipse may grossly underestimate the actual region of uncertainty. Examples are the NORESS solution (1) for event 361-11 (Table 12b) and the FINESA solution (2) for 359-12 (Table 13b) where the F-statistic solutions indicate no uncertainty. This occurs because each event has one P and one S arrival time that provide an unambiguous estimate of event distance and associated azimuth measurements that are identical (Tables 12 and 13a). As a result, the computed \underline{r}_w^2 , s_s^2 and confidence dimensions are zero. Though not quite as extreme, the F-statistic ellipse (4) of events 361-12, 351-13, and 363-21 (Figures 15 - 17a) appear underestimated because they fail to include the independent event location. Again, the reason is a misleading consistency

among the few available data.

In most cases, the F-statistic confidence ellipse appears overestimated. As discussed by Evernden (1969), this problem results because s_s^2 and F_p become large as the N approaches M . Examples include the one-array (1 and 2) and arrival time only (3) ellipses for events 361-11 (Figure 12a), 359-12 (13a) and 359-14 (14a). For example, though the lengths of the semi-major axes for solutions (2) and (3) of event 361-11 are about 600 and 900 km, respectively, the ΔL is less than 10% as large. When $N = M$, the F-statistic ($F_p(M,0)$) is undefined. Therefore, no confidence bounds may be placed on the location. The arrival-time only solutions for events 350-16, 351-13, 363-21 (Figures 11, 16 and 17a) suffer from this problem.

The above-described problems can be mitigated by incorporating *a priori* information from location solutions in a region of interest into the calculation of K-weighted confidence bounds. The *a priori* variance scale factor s_K^2 and associated measure of uncertainty K which contribute to the K-weighted ellipse are computed from the s_s^2 of past events in a selected area. Five of the events examined in this study are concentrated in the area between 150 and 275 km east of FINESA (351-13, 359-12, 359-14, 361-11 and 361-12). We use s_s^2 from solutions (4) (i.e., solutions using all available data) for the four events that occurred on days 359 and 361 to demonstrate the derivation of s_K^2 and K . The very low s_s^2 for the fifth event in the vicinity (351-13) indicates that the data for this event were exceptionally accurate and uncharacteristic of the other four events. We therefore exclude it from the following analysis so as to avoid biasing the small sample of s_s^2 .

The s_K^2 is the mean of the s_s^2 . Using the s_s^2 from locations (4) in Tables 12 through 15b, $s_K^2 = 2.4$. The fact that s_K^2 is not unity suggests that the assigned variances were on the average underestimated (see equation 4). In an operational situation, it might be desirable to continually update the variance matrix, V_d , so as to keep the s_K^2 close to unity. The mean and standard deviation of the quantity $(1/s_s)$ are 0.70 and 0.17. A standard deviation of 24% corresponds to a value of K of about 8 (see Jordan and Sverdrup, 1981, Figure 3).

The s_K^2 and K are inserted into equations (12) and (13) to derive a new *a posteriori* estimate, s_e^2 , for the variance scale factor and new confidence coefficient κ_p^2 . The dimensions of the

resulting K-weighted solutions are given in the columns marked "K" in Tables/Figures 12 - 15b. The same K and s_K^2 were applied in all one and two array solutions. Though, the s_K^2 and σ) and K are expected to be area-specific values, we have applied these values to the other three events shown in Tables/Figures 11, 16 and 17b.

The advantages of the K-weighted ellipses are obvious from the figures. All K-weighted solutions have finite confidence bounds. The reason is evident from examination of equations (12) and (13). As long as $K + N > M$, both s_e^2 and the confidence coefficient κ_p^2 will be finite. Furthermore, the ellipses that appeared greatly overestimated by the F-statistic approach have been reduced by including the *a priori* information. Most importantly, all independent locations now fall within or on the K-weighted confidence bounds derived from all subsets of data (single array, two array, arrival time only, and time plus azimuth). Thus even with the few data examined here, the Jordon and Sverdrup (1981) method provides consistent and apparently realistic measures of the solution accuracy.

Table 13a

Data for Event 359-12, 1985.					
Array	Datum	t (min:sec)	σ_t (sec)	α	σ_α
NOR	Pn	6:30.3	0.8	80°	6°
NOR	Sn	8:05.5	2.7	99°	6°
NOR	S	8:54.1		82°	6°
NOR	Lg	9:00.5	2.9	99°	8°
FIN	Pg	4:51.4	0.8	109°	15°
FIN	P	4:56.2		123°	12°
FIN	Lg	5:12.8	1.5	109°	11°
FIN	S	5:20.0		111°	17°

Table 13b

Locations for Event 359-12, 1985 (Figure 13).								
# Data		Latitude	Longitude	s_s^2	Semi-major axis (km)	Semi-minor axis (km)	ΔL (km)	
Noress t	Finess α							
					F / K	F / K		
		Independent	60.9°	29.3°				
(1)	3	3	59.30°	28.86°	2.46	325 / 228	85 / 59	180
(2)		2	60.91°	29.09°	0.00	0 / 94	0 / 47	11
(3)	3	2	61.04°	29.43°	8.53	493 / 180	113 / 41	17
(4)	3	3	61.10°	29.09°	4.16	108 / 85	48 / 38	25

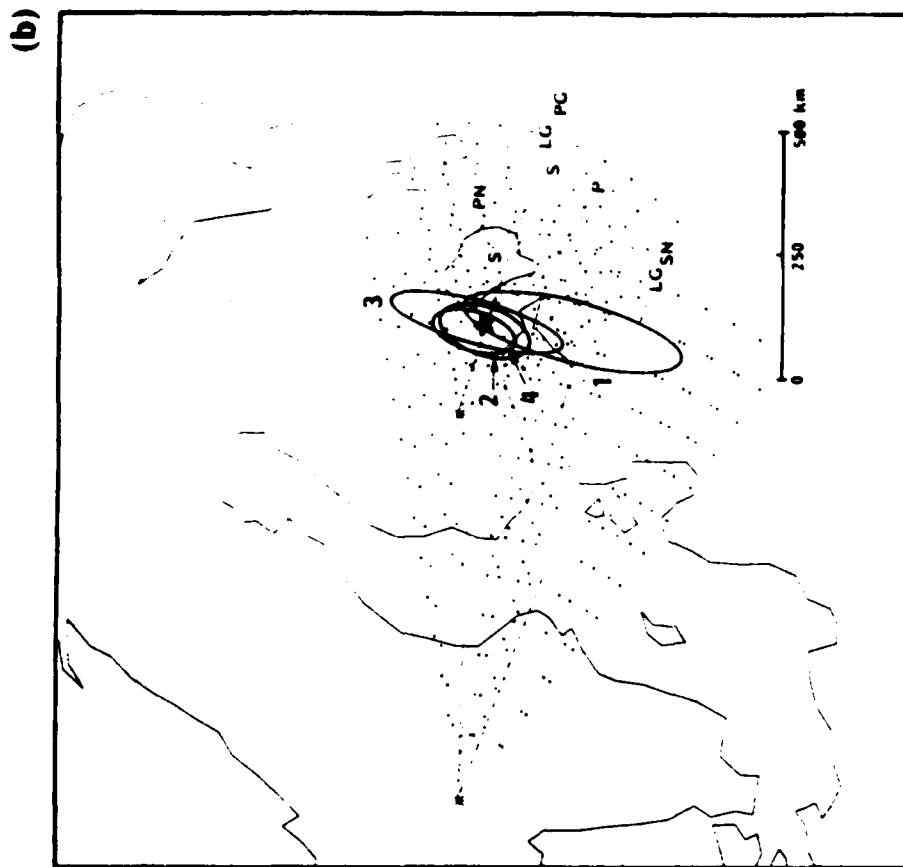
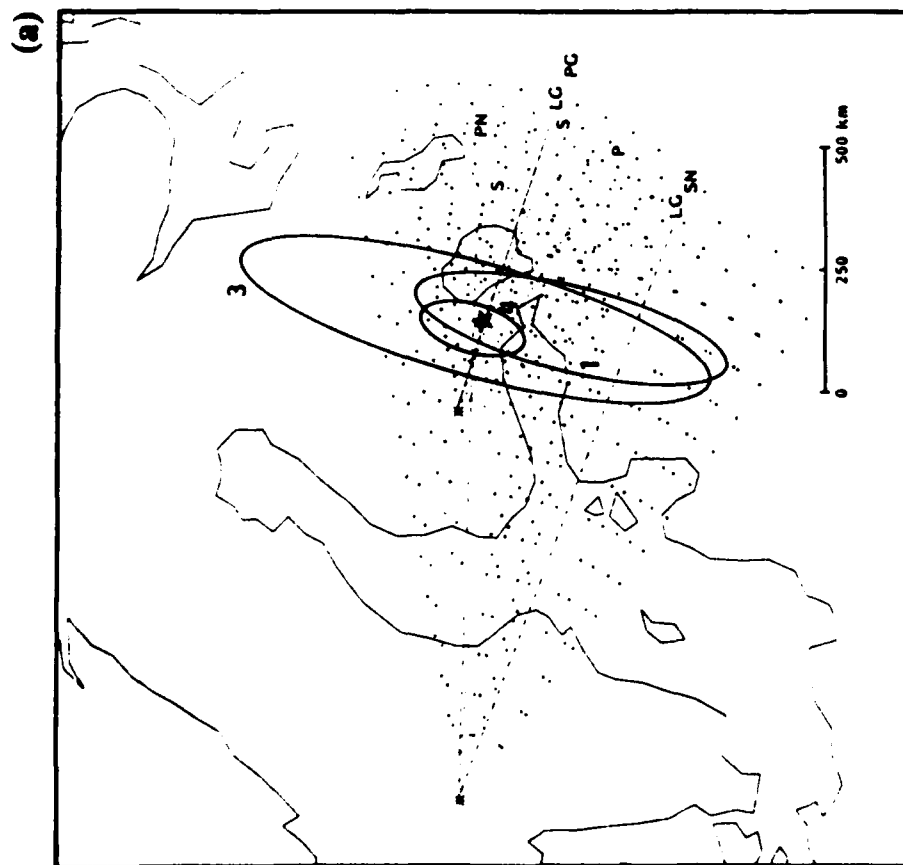


Figure 13. Solutions for event 359-12. (a) F-statistic confidence ellipse, (b) K-weighted confidence ellipses. (Tables 13a and b).

Table 14a

Data for Event 359-14, 1985.					
Array	Datum	t (min:sec)	σ_t (sec)	α	σ_α
NOR	Pn	20:07.4	0.8	97°	8°
NOR	P	20:12.4		86°	21°
NOR	Sn	21:42.6	2.9	86°	11°
NOR	Lg	22:31.8	2.8	83°	10°
FIN	Pg	18:28.7	0.8	120°	9°
FIN	N	18:34.5		115°	5°
FIN	Lg	18:50.0	1.5	101°	9°
FIN	S	18:59.7		121°	14°

Table 14b

Locations for Event 359-14, 1985 (Figure 14).									
		# Data		Latitude	Longitude	s_f^2	Semi-major axis (km) F / K	Semi-minor axis (km) F / K	ΔL (km)
		Noress t	Finess α						
Independent									
(1)	3	3		59.60°	28.53°	1.77	398 / 316	71 / 56	
(2)			2 2	60.89°	29.05°	2.34	282 / 68	206 / 50	
(3)	3		2	61.29°	29.08°	3.61	865 / 412	74 / 35	
(4)	3	3	2 2	61.05°	28.90°	2.37	59 / 53	36 / 32	

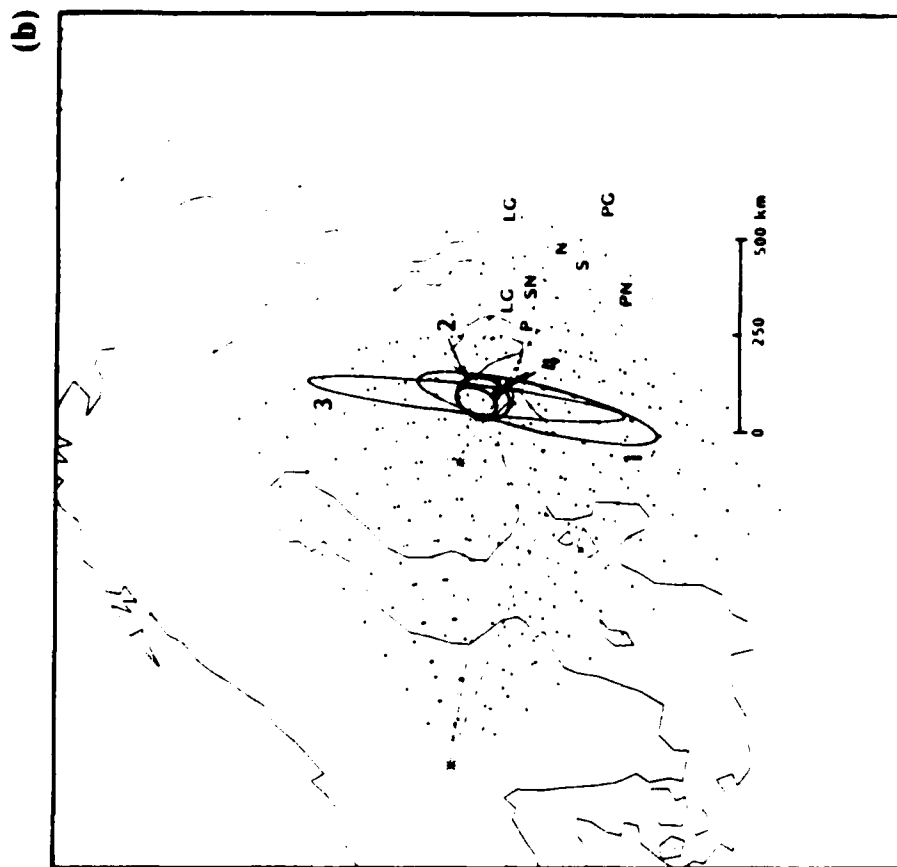
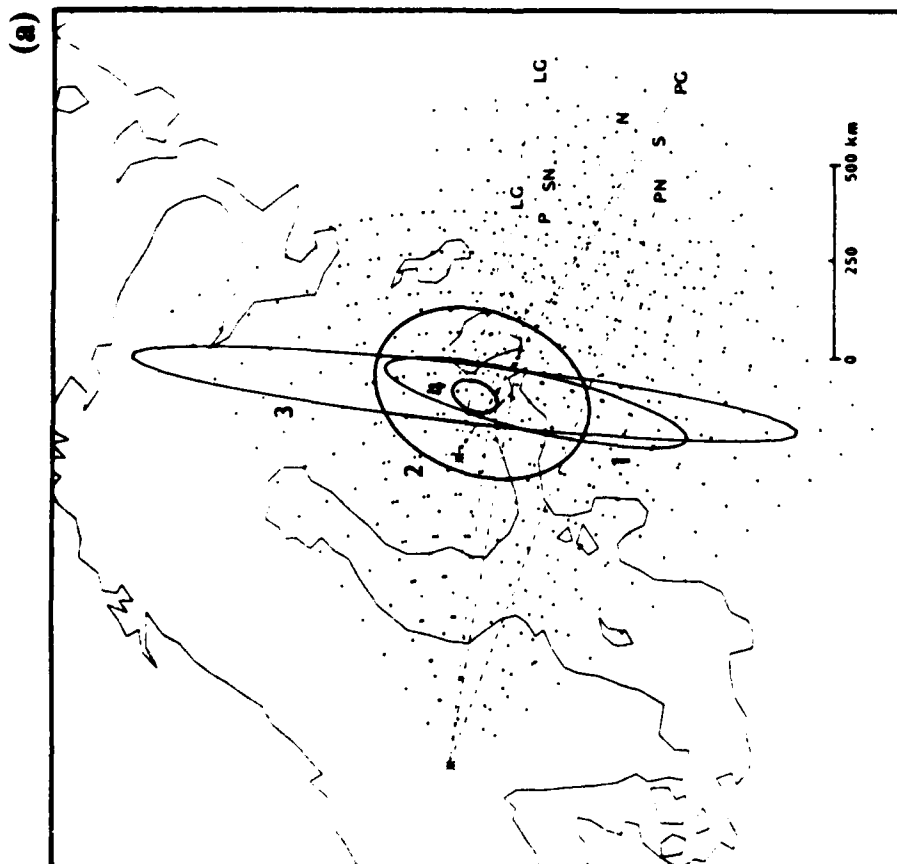


Figure 14. Solutions for event 359-14. (a) F-statistic confidence ellipse, (b) K-weighted confidence ellipses. (Tables 14a and b).

Table 15a

Data for Event 361-12, 1985.					
Array	Datum	t (min:sec)	σ_t (sec)	α	σ_α
NOR	Pn	18:10.5	0.8	81°	11°
NOR	Sn	19:44.4	2.6	94°	4°
NOR	S	19:49.5		86°	6°
NOR	Lg	20:31.8	2.0	98°	6°
NOR	S	20:37.1		100°	5°
NOR	N	23:06.1		96°	3°
FIN	Pg	16:51.2	0.8	148°	8°
FIN	P	16:58.4		150°	14°
FIN	Lg	17:22.4	1.5	159°	8°
FIN	S	17:28.3		148°	8°

Table 15b

Locations for Event 361-12, 1985 (Figure 15).								
# Data		Latitude	Longitude	s^2_s	Semi-major axis (km)	Semi-minor axis (km)	ΔL (km)	
Noress t	Finess α							
					F / K	F / K		
		Independent	59.4°	28.5°				
(1)	3	3						
			59.11°	27.79°	2.69	260 / 176	45 / 67	52
(2)		2	2					
			59.41°	28.06°	0.88	240 / 91	126 / 48	25
(3)	3		2					
			59.38°	27.95°	3.03	76 / 38	46 / 23	31
(4)	3	3	2	2				
			59.38°	27.96°	1.35	29 / 31	18 / 19	31

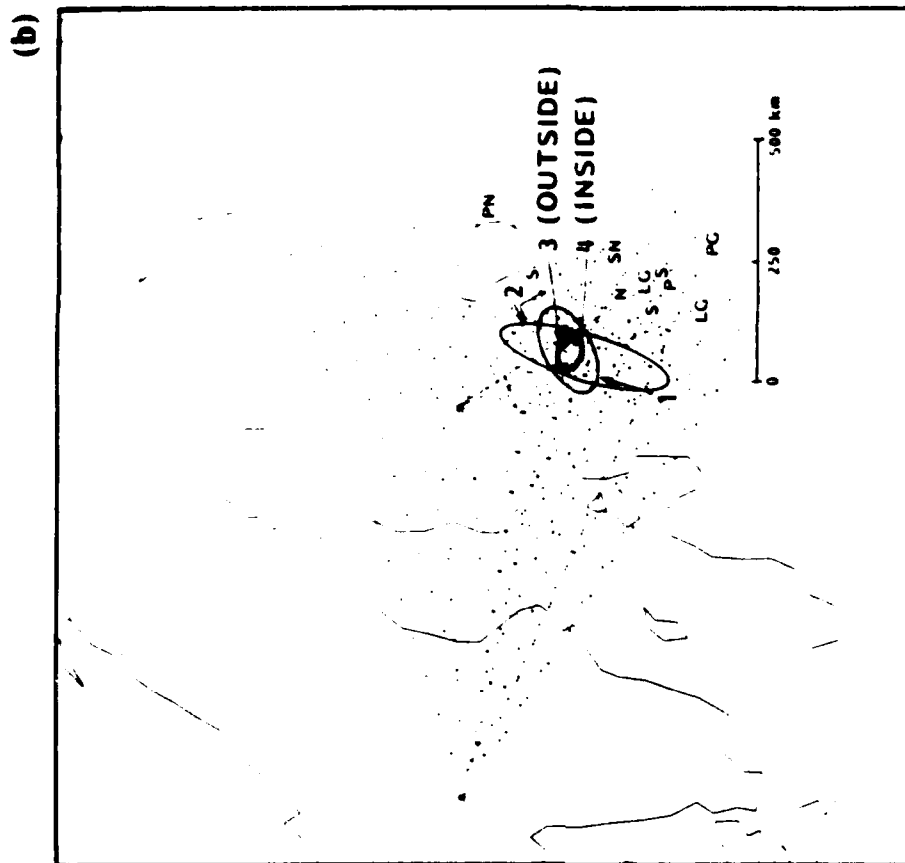
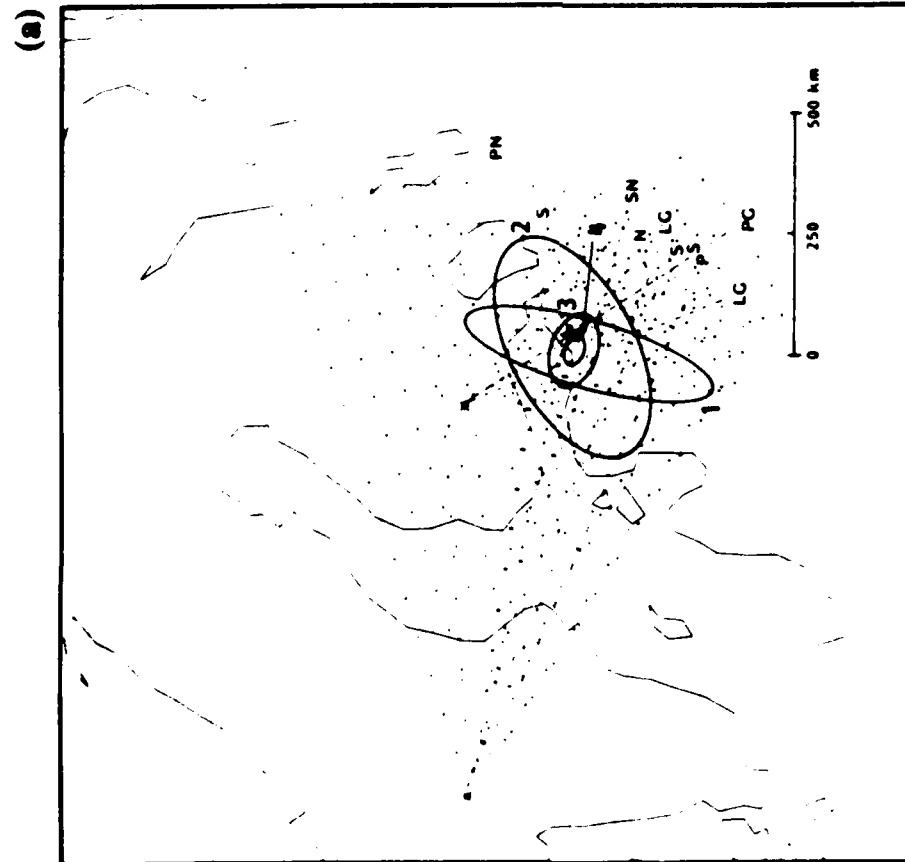


Figure 15. Solutions for event 361-12. (a) F-statistic confidence ellipse, (b) K-weighted confidence ellipses. (Tables 15a and b).

Table 16a

Data for Event 351-13, 1985.					
Array	Datum	t (min:sec)	σ_t (sec)	α	σ_α
NOR	Pn	10:38.2	0.8	81°	15°
FIN	Pg	9:04.0	0.8	105°	10°
FIN	P	9:08.7		80°	17°
FIN	Lg	9:29.8	1.5	103°	12°
FIN	N	9:34.4		79°	5°
FIN	S	9:39.4		95°	25°

Table 16b

Locations for Event 351-13, 1985 (Figure 16).									
	# Data		Latitude	Longitude	s_s^2	Semi-major axis (km) F / K	Semi-minor axis (km) F / K	ΔL (km)	
	Noress t	Finess α							
	Independent		61.1°	30.2°					
(2)		2 2	60.94°	29.80°	0.02	36 / 94	18 / 47	28	
(3)	1	2	60.80°	29.70°	0.00	∞ / 173	∞ / 36	43	
(4)	1 1	2 2	60.90°	29.83°	0.04	15 / 76	6 / 30	30	

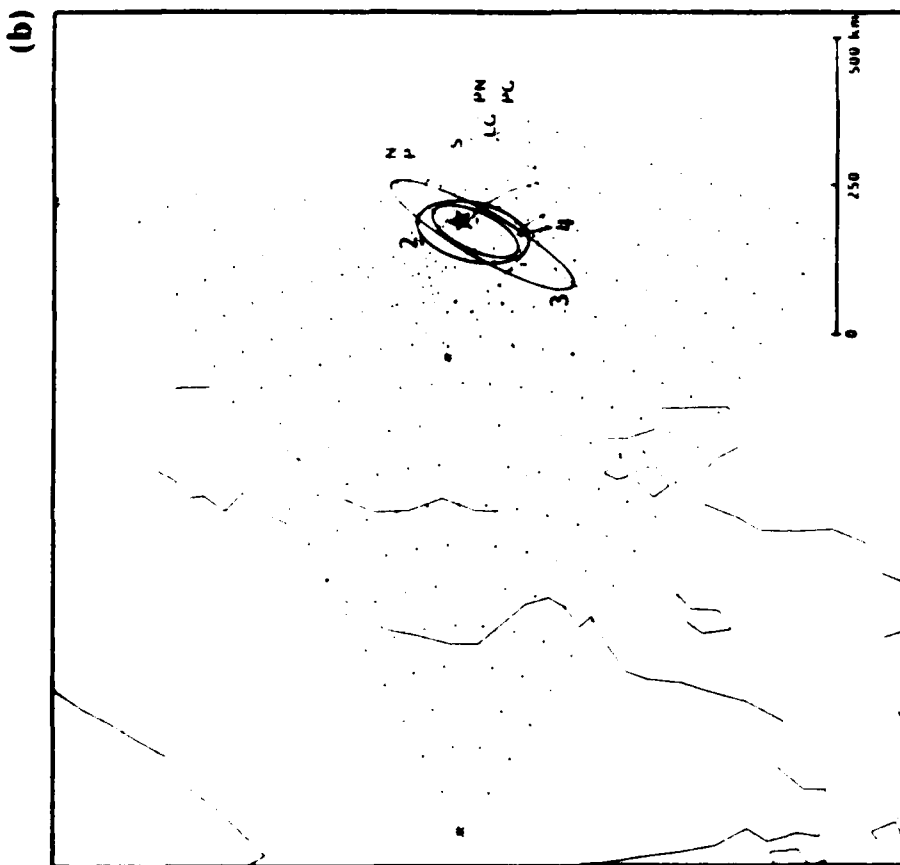
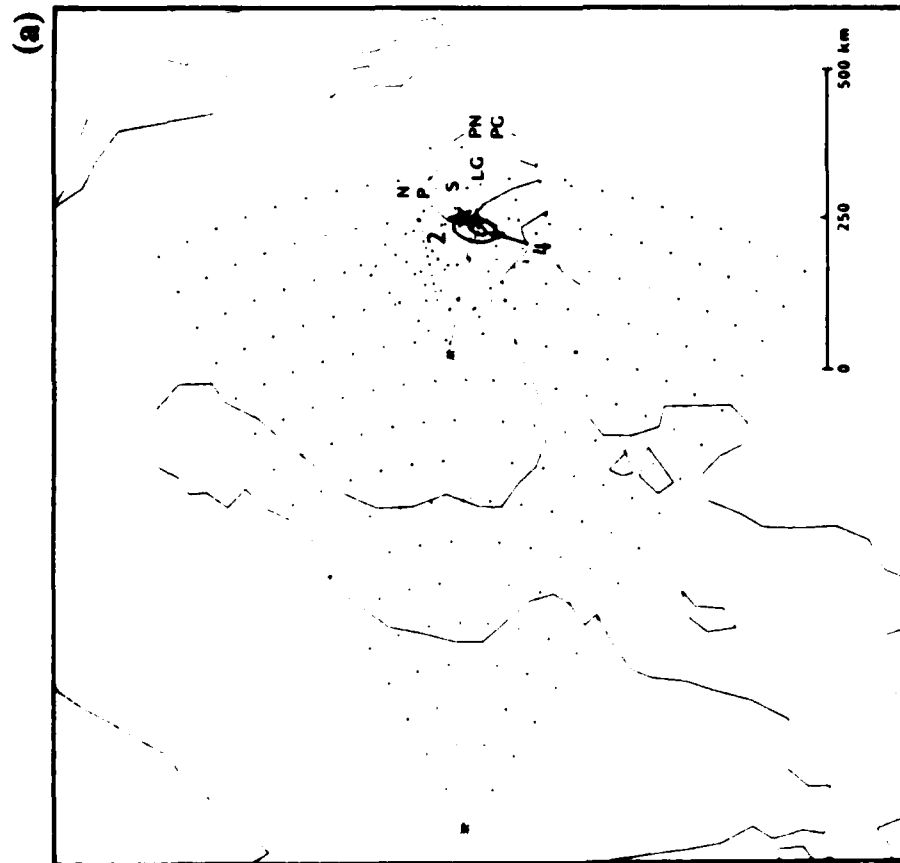


Figure 16. Solutions for event 351-13. (a) F-statistic confidence ellipse, (b) K-weighted confidence ellipses. (Tables 16a and b).

Table 17a

Data for Event 363-21, 1985.					
Array	Datum	t (min:sec)	σ_t (sec)	α	σ_α
NOR	Pn	40:58.3	0.8	348°	10°
NOR	P	41:05.2		356°	11°
NOR	P	41:10.8		348°	8°
NOR	Sn	43:11.6	1.5	352°	11°
NOR	S	43:29.0		1°	5°
NOR	S	43:33.7		351°	9°
FIN	Pn	41:17.2	0.8	347°	26°
FIN	P	41:21.7		354°	15°

Table 17b

Locations for Event 363-21, 1985 (Figure 17).								
		# Data		Latitude	Longitude	s^2	Semi-major axis (km) F / K	Semi-minor axis (km) F / K
Noress t	Finess α	Noress t	Finess α					
		Independent		73.2°	5.7°			
(1)	2	2		73.26°	3.68°	0.07	495 / 642	50 / 66
(3)	2		1	73.35°	4.83°	0.00	∞ / 90	∞ / 49
(4)	2	2	1 1	73.35°	4.82°	0.11	26 / 74	15 / 41

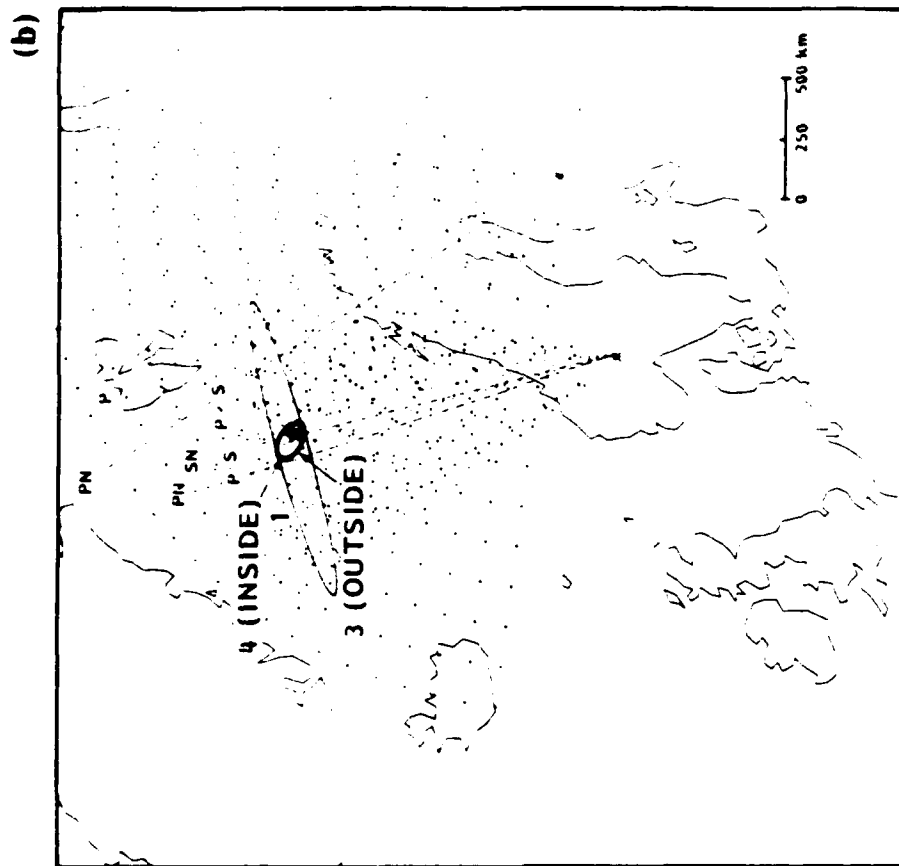
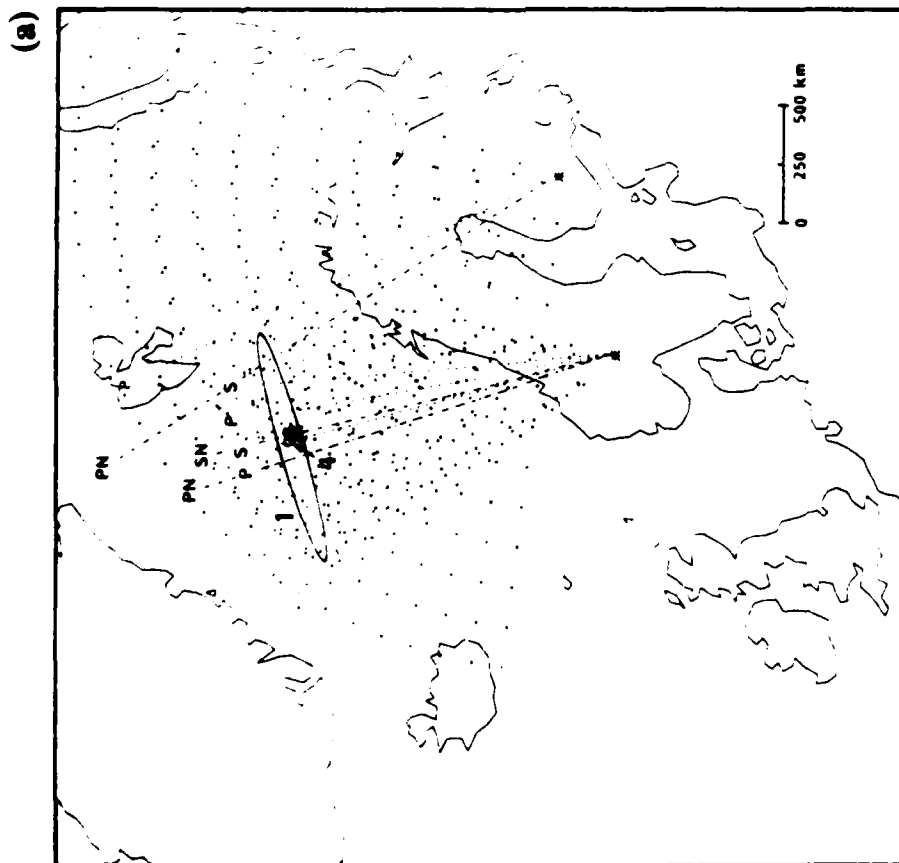


Figure 17. Solutions for event 363-21. (a) F-statistic confidence ellipse, (b) K-weighted confidence ellipses. (Tables 17a and b).

DISCUSSION

We have shown that extending location algorithms to formally include azimuth estimates provides a significant improvement in the location solution for regional events detected by one or a few arrays. Azimuth data have been neglected in location estimation because they are too uncertain (e.g., from polarization analysis of three-component data) or because they are not important when the event is far away (most arrays emphasize teleseismic monitoring). But the NORESS-type arrays are designed to monitor small regional events that are detected by only a few stations or arrays, and in this situation the azimuth estimates provide a powerful constraint on the solution and the estimates for the confidence ellipsoid.

The particular location algorithm we have chosen is that of Jordan and Sverdrup (1981) which is especially well-suited to this problem. The key feature is that it includes the capability to weight the relative contribution to the confidence ellipsoid of *a priori* knowledge of the data variances (developed from past experience) and the solution residuals. It also provides a basis for refining the validity of the *a priori* variances, and therefore the confidence ellipsoid, as experience is accumulated with events in a particular region.

The relative contribution of arrival time data and azimuth data to the solution and the dimensions of the confidence ellipsoid depend on the data variances. We have implemented a procedure in which the values of these variances depend on the character of the particular signal (signal/noise, f-k solution quality, beam resolution). But the algorithm for computing the variances includes some arbitrary factors whose validity can only be assessed with experience. Thus, we expect to refine the basis for assigning the variances themselves, as well as the parameters that weight their contribution to the confidence ellipsoid, as experience is accumulated. The examples presented in this study indicate that our initial selection is rather good.

There are some potentially important aspects of the problem that were not examined in any detail in this initial study. One is the value of including azimuth estimates from secondary phases with useless arrival times (e.g., a detection in the P coda). For the examples presented here, the secondary phase azimuths appear to be as accurate as those for primary phases. If all azimuth estimates are viewed as equally unbiased samples of a random population of estimates

of the true azimuth, including these secondary azimuth estimates would improve the solution. More experience and further study is needed to decide how reasonable this assumption seems to be.

Finally, we plan a straightforward extension of the location estimation procedure to add the capability for 'master event' location. The formulation presented assumes that the elements of the residual vector (r) are due to random, zero mean processes. This does not account for systematic bias due to, for example, systematic errors in the earth model. Bias can be substantially reduced by computing locations relative to a nearby 'master event' which is well-located (e.g., Douglas, 1967; Jordan and Sverdrup, 1981).

ACKNOWLEDGEMENTS

We gratefully acknowledge William L. Rodi (S-CUBED) for providing us with his location code which we modified to become *TTAZLOC*. Our colleague Anne Suteau-Henson implemented the signal processing code and provided the detection data and standard deviations used in this paper. This code was based on the NORSAR program RONAPP (kindly provided by the NORSAR staff). Data were furnished by NORSAR, the SCARS Project at Sandia National Laboratories, the Center for Seismic Studies, and Helsinki University. Nancy Woltman, Donna Williams and Marcia Brown were responsible for the preparation of the manuscript and figures.

REFERENCES

- Aki, K. and P. G. Richards (1980). Quantitative Seismology, W. H. Freeman and Company, San Francisco, pp 641 - 719.
- Bungum, H., S. Mykkeltveit, and T. Kvaerna (1985). Seismic noise in Fennoscandia, with emphasis on high frequencies, *Bull. Seism. Soc. Am.* **75**, 1489-1513.
- Douglas, A. (1967). Joint epicenter determination, *Nature* **215**, 47 - 48.
- Evernden, J. F. (1969). Precision of epicenters obtained by small numbers of world-wide stations, *Bull. Seism. Soc. Am.* **59**, 1365 - 1398.
- Flinn, E. A. (1965). Confidence regions and error determinations for seismic event location, *Rev. Geophys.* **3**, 157 - 185.
- Geiger, L. (1910). Herdbestimmung bei erdbeben ans den ankunftszeiten, *K. Gessel. Wiss. Goett.* **4**, 331 - 349.
- Gjoystdal, H., E. S. Husebye, and D. Rieber-Mohn (1973). One-array and two-array location capabilities, *Bull. Seism. Soc. Am.* **63**, 549-569.
- Jordon, T. H. and K. A. Sverdrup (1981). Teleseismic location techniques and their application to earthquake clusters in the South-Central Pacific, *Bull. Seism. Soc. Am.* **71**, 1105 - 1130.
- Julian, B. R. (1973). Extension of standard event location procedures, *Seismic Discrimination SATS*, Lincoln Laboratory, Massachusetts Institute of Technology, DDC AD-766559.
- Klein, F. (1978). Hypocenter location program HYPOINVERSE, *U. S. Geol. Surv. Open-File Report 78 - 694*, 113 pp.

Korhonen, H., S. Pirhonen, F. Ringdal, S. Mykkeltveit, T. Kvaerna, P. S. Larsen, and R. Paulsen (1987). The FINESA array and preliminary results of data analysis, Report S-16, Institute of Seismology, University of Helsinki.

Kvaerna, T. and D. J. Doornbos (1986). An integrated approach to slowness analysis with arrays and three-component seismometers. In NORSAR Scientific Report 2-35/86, Kjeller, Norway

Mykkeltveit S., K. Astebol, D. J. Doornbos, and E. S. Husebye (1983). Seismic array configuration optimization, *Bull. Seism. Soc. Am.* 73, 173 - 186.

Mykkeltveit S. and Bungum (1984). Processing of regional seismic events using data from small-aperture arrays, *Bull. Seism. Soc. Am.* 74, 2313 - 2333.

Rivers, D. W., J. A. Burnetti, and A. C. Chang (1981). Use of back azimuth measurements in seismic event location with regional data. *VELA Seismic Center Technical Report 81 - 17*, 80 pp.

Romney, C. F. (1985). VELA Overview. The early years of the seismic research program, in *The VELA Program*, A. U. Kerr Editor, Defense Advanced Research Projects Agency pp 38 - 65.

Shlien, S. and M. N. Toksoz (1973). Automatic event detection and location capabilities of large aperture seismic arrays, *Bull. Seism. Soc. Am.* 63, 1275 - 1288.

DISTRIBUTION LIST

Dr. Monem Abdel-Gawad
Rockwell International Science Center
1049 Camino Dos Rios
Thousand Oaks, CA 91360

Professor Keiiti Aki
Center for Earth Sciences
University of Southern California
University Park
Los Angeles, CA 90089-0741

Professor Shelton S. Alexander
Geosciences Department
403 Deike Building
The Pennsylvania State University
University Park, PA 16802

Professor Charles B. Archambeau
Cooperative Institute for Research in
Environmental Sciences
University of Colorado
Boulder, CO 80309

Dr. Thomas C. Bache Jr.
Science Applications Int'l Corp.
10210 Campus Point Drive
San Diego, CA 92121

Dr. James Bulau
Rockwell International Science Center
1049 Camino Dos Rios
P.O. Box 1085
Thousand Oaks, CA 91360

Dr. Douglas R. Baumgardt
Signal Analysis and Systems Division
ENSCO, Inc.
5400 Port Royal Road
Springfield, VA 22151-2388

Dr. S. Bratt
Science Applications Int'l Corp.
10210 Campus Point Drive
San Diego, CA 92121

Professor John Ebel
Department of Geology & Geophysics
Boston College
Chestnut Hill, MA 02167

Woodward-Clyde Consultants
Attn: Dr. Lawrence J. Burdick
Dr. Jeff Barker
P.O. Box 93245
Pasadena, CA 91109-3245 (2 copies)

Dr. Roy Burger
1221 Serry Rd.
Schenectady, NY 12309

Professor Robert W. Clayton
Seismological Laboratory
Division of Geological and Planetary
Sciences
California Institute of Technology
Pasadena, CA 91125

Dr. Vernon F. Cormier
Earth Resources Laboratory
Department of Earth, Atmospheric and
Planetary Sciences
Massachusetts Institute of Technology
42 Carleton Street
Cambridge, MA 02142

Professor Anton M. Dainty
Earth Resources Laboratory
Department of Earth, Atmospheric and
Planetary Sciences
Massachusetts Institute of Technology
42 Carleton Street
Cambridge, MA 02142

Dr. Zoltan A. Der
Teledyne Geotech
314 Montgomery Street
Alexandria, VA 22314

Prof. Adam Dziewonski
Hoffman Laboratory
Harvard University
20 Oxford St.
Cambridge, MA 02138

Professor John Ferguson
Center for Lithospheric Studies
The University of Texas at Dallas
P.O. Box 830688
Richardson, TX 75083-0688

Dr. Jeffrey W. Given
Sierra Geophysics
11255 Kirkland Way
Kirkland, WA 98033

Prof. Roy Greenfield
Geosciences Department
403 Deike Building
The Pennsylvania State University
University Park, PA 16802

Professor David G. Harkrider
Seismological Laboratory
Division of Geological and Planetary
Sciences
California Institute of Technology
Pasadena, CA 91125

Professor Donald V. Helmberger
Seismological Laboratory
Division of Geological and Planetary
Sciences
California Institute of Technology
Pasadena, CA 91125

Professor Eugene Herrin
Institute for the Study of Earth & Man
Geophysical Laboratory
Southern Methodist University
Dallas, TX 75275

Professor Robert B. Herrmann
Department of Earth and Atmospheric
Sciences
Saint Louis University
Saint Louis, MO 63156

Professor Lane R. Johnson
Seismographic Station
University of California
Berkeley, CA 94720

Professor Thomas H. Jordan
Department of Earth, Atmospheric and
Planetary Sciences
Massachusetts Institute of Technology
Cambridge, MA 02139

Dr. Alan Kafka
Department of Geology & Geophysics
Boston College
Chestnut Hill, MA 02167

Professor Charles A. Langston
Geosciences Department
403 Deike Building
The Pennsylvania State University
University Park, PA 16802

Professor Thorne Lay
Department of Geological Sciences
1006 C.C. Little Building
University of Michigan
Ann Arbor, MI 48109-1063

Dr. George R. Mellman
Sierra Geophysics
11255 Kirkland Way
Kirkland, WA 98033

Professor Brian J. Mitchell
Department of Earth and Atmospheric
Sciences
Saint Louis University
Saint Louis, MO 63156

Professor Thomas V. McEvilly
Seismographic Station
University of California
Berkeley, CA 94720

Dr. Keith L. McLaughlin
Teledyne Geotech
314 Montgomery Street
Alexandria, VA 22314

Professor Otto W. Nuttli
Department of Earth and Atmospheric
Sciences
Saint Louis University
Saint Louis, MO 63156

Professor Paul G. Richards
Lamont-Doherty Geological Observatory
of Columbia University
Palisades, NY 10964

Dr. Norton Rimer
S-Cubed
A Division of Maxwell Laboratory
P.O. 1620
La Jolla, CA 92038-1620

Professor Larry J. Ruff
Department of Geological Sciences
1006 C.C. Little Building
University of Michigan
Ann Arbor, MI 48109-1063

Professor Charles G. Sammis
Center for Earth Sciences
University of Southern California
University Park
Los Angeles, CA 90089-0741

Dr. David G. Simpson
Lamont-Doherty Geological Observatory
of Columbia University
Palisades, NY 10964

Dr. Jeffrey L. Stevens
S-CUBED,
A Division of Maxwell Laboratory
P.O. Box 1620
La Jolla, CA 92038-1620

Professor Brian Stump
Institute for the Study of Earth
and Man
Geophysical Laboratory
Southern Methodist University
Dallas, TX 75275

Professor Ta-liang Teng
Center for Earth Sciences
University of Southern California
University Park
Los Angeles, CA 90089-0741

Dr. R. B. Tittmann
Rockwell International Science Center
1049 Camino Dos Rios
P.O. Box 1085
Thousand Oaks, CA 91360

Professor M. Nafi Toksoz
Earth Resources Laboratory
Department of Earth, Atmospheric and
Planetary Sciences
Massachusetts Institute of Technology
42 Carleton Street
Cambridge, MA 02142

Professor Terry C. Wallace
Department of Geosciences
Building #11
University of Arizona
Tucson, AZ 85721

Prof. John H. Woodhouse
Hoffman Laboratory
Harvard University
20 Oxford St.
Cambridge, MA 02138

Dr. G. Blake
US Dept of Energy/DP 331
Forrestal Building
1000 Independence Ave.
Washington, D.C. 20585

Dr. Michel Bouchon
Universite Scientifique et
Medicale de Grenoble
Laboratoire de Geophysique
Interne et Tectonophysique
I.R.I.G.M.-B.P. 68
38402 St. Martin D'Herès
Cedex FRANCE

Dr. Hilmar Bungum
NTNF/NORSAR
P.O. Box 51
Norwegian Council of Science,
Industry and Research, NORSAR
N-2007 Kjeller, NORWAY

Dr. Alan Douglas
Ministry of Defense
Blacknest, Brimpton, Reading RG7-4RS
UNITED KINGDOM

Professor Peter Harjes
Institute for Geophysics
Rhur University
Bochum
P.O. Box 102148
4630 Bochum 1
FEDERAL REPUBLIC OF GERMANY

Dr. James Hannon
Lawrence Livermore National Laboratory
P.O. Box 808
Livermore, CA 94550

Dr. E. Husebye
NTNF/NORSAR
P.O. Box 51
N-2007 Kjeller, NORWAY

Dr. Arthur Lerner-Lam
Lamont-Doherty Geological Observatory
of Columbia University
Palisades, NY 10964

Mr. Peter Marshall
Procurement Executive
Ministry of Defense
Blacknest, Brimpton, Reading RG7-4RS
UNITED KINGDOM

Dr. B. Massinon
Societe Radiomana
27, Rue Claude Bernard
75005, Paris, FRANCE

Dr. Pierre Mechler
Societe Radiomana
27, Rue Claude Bernard
75005, Paris, FRANCE

Mr. Jack Murphy
S-CUBED
Reston Geophysics Office
11800 Sunrise Valley Drive
Suite 1212
Reston, VA 22091

Dr. Svein Mykkeltveit
NTNF/NORSAR
P.O. Box 51
N-2007 Kjeller, NORWAY

Dr. Carl Newton
Los Alamos National Laboratory
P.O. Box 1663
Mail Stop C 335, Group ESS3
Los Alamos, NM 87545

Dr. Peter Basham
Earth Physics Branch
Department of Energy and Mines
1 Observatory Crescent
Ottawa, Ontario
CANADA K1A 0Y3

Professor J. A. Orcutt
Geological Sciences Division
Univ. of California at San Diego
La Jolla, CA 92093

Dr. Frank F. Pilotte
Director of Geophysics
Headquarters Air Force Technical
Applications Center
Patrick AFB, Florida 32925-6001

Professor Keith Priestley
University of Nevada
Mackay School of Mines
Reno, Nevada 89557

Mr. Jack Raelin
USGS - Geology, Rm 3C136
Mail Stop 928 National Center
Reston, VA 22092

Dr. Frode Ringdal
NTNF/NORSAR
P.O. Box 51
N-2007 Kjeller, NORWAY

Dr. George H. Rothe
Chief, Research Division
Geophysics Directorate
Headquarters Air Force Technical
Applications Center
Patrick AFB, Florida 32925-6001

Dr. Alan S. Ryall, Jr.
Center for Seismic Studies
1300 North 17th Street
Suite 1450
Arlington, VA 22209-2308

Dr. Jeffrey L. Stevens
S-CUBED,
A Division of Maxwell Laboratory
P.O. Box 1620
La Jolla, CA 92038-1620

Dr. Lawrence Turnbull
OSWR/NED
Central Intelligence Agency
CIA, Room 5G48
Washington, DC 20505

Professor Steven Grand
Department of Geology
245 Natural History Bldg
1301 West Green Street
Urbana, IL 61801

DARPA/PM
1400 Wilson Boulevard
Arlington, VA 22209

Defense Technical Information Center
Cameron Station
Alexandria, VA 22314 (12 copies)

Defense Intelligence Agency
Directorate for Scientific and
Technical Intelligence
Washington, D.C. 20301

Defense Nuclear Agency
Shock Physics Directorate/SS
Washington, D.C. 20305

Defense Nuclear Agency/SPSS
ATTN: Dr. Michael Shore
6801 Telegraph Road
Alexandria, VA 22310

AFOSR/NPG
ATTN: Director
Bldg 410, Room C222
Bolling AFB, Washington, D.C. 20332

AFTAC/CA (STINFO)
Patrick AFB, FL 32925-6001

AFWL/NTESC
Kirtland AFB, NM 87171

U.S. Arms Control & Disarmament Agency
ATTN: Mrs. M. Hoinkes
Div. of Multilateral Affairs, Rm 5499
Washington, D.C. 20451

U.S. Geological Survey
ATTN: Dr. T. Hanks
National Earthquake Research Center
345 Middlefield Road
Menlo Park, CA 94025

SRI International
333 Ravensworth Avenue
Menlo Park, CA 94025

Center for Seismic Studies
ATTN: Dr. C. Romney
1300 North 17th Street
Suite 1450
Arlington, VA 22209 (3 copies)

Dr. Robert Blandford
DARPA/GSD
1400 Wilson Boulevard
Arlington, VA 22209-2308

Ms. Ann Kerr
DARPA/GSD
1400 Wilson Boulevard
Arlington, VA 22209-2308

Dr. Ralph-Alewine III
DARPA/GSD
1400 Wilson Boulevard
Arlington, VA 22209-2308

Mr. Edward Giller
Pacific Sierra Research Corp.
1401 Wilson Boulevard
Arlington, VA 22209

Science Horizons, Inc.
Attn: Dr. Bernard Minster
Dr. Theodore Cherry
710 Encinitas Blvd., Suite 101
Encinitas, CA 92024 (2 copies)

Dr. Jack Evernden
USGS - Earthquake Studies
345 Middlefield Road
Menlo Park, CA 94025

Dr. Lawrence Braile
Department of Geosciences
Purdue University
West Lafayette, IN 47907

Dr. G.A. Bollinger
Department of Geological Sciences
Virginia Polytechnical Institute
21044 Derring Hall
Blacksburg, VA 24061

Dr. L. Sykes
Lamont Doherty Geological Observatory
Columbia University
Palisades, NY 10964

Dr. S.W. Smith
Geophysics Program
University of Washington
Seattle, WA 98195

Dr. L. Timothy Long
School of Geophysical Sciences
Georgia Institute of Technology
Atlanta, GA 30332

Dr. N. Biswas
Geophysical Institute
University of Alaska
Fairbanks, AK 99701

Dr. Freeman Gilbert
Institute of Geophysics &
Planetary Physics
Univ. of California at San Diego
P.O. Box 109
La Jolla, CA 92037

Dr. Pradeep Talwani
Department of Geological Sciences
University of South Carolina
Columbia, SC 29208

University of Hawaii
Institute of Geophysics
Attn: Dr. Daniel Walker
Honolulu, HI 96822

Dr. Donald Forsyth
Department of Geological Sciences
Brown University
Providence, RI 02912

Dr. Jack Oliver
Department of Geology
Cornell University
Ithaca, NY 14850

Dr. Muawia Barazangi
Geological Sciences
Cornell University
Ithaca, NY 14853

Rondout Associates
Attn: Dr. George Sutton
Dr. Jerry Carter
Dr. Paul Pomeroy
P.O. Box 224
Stone Ridge, NY 12484 (3 copies)

Dr. M. Sorrells
Geotech/Teledyne
P.O. Box 28277
Dallas, TX 75228

Dr. Bob Smith
Department of Geophysics
University of Utah
1400 East 2nd South
Salt Lake City, UT 84112

Dr. Anthony Gangi
Texas A&M University
Department of Geophysics
College Station, TX 77843

Dr. Gregory B. Young
ENSCO, Inc.
5400 Port Royal Road
Springfield, CA 22151

Dr. Ben Menaheim
Weizman Institute of Science
Rehovot, ISRAEL 951729

Weidlinger Associates
Attn: Dr. Gregory Wojcik
620 Hansen Way, Suite 100
Palo Alto, CA 94304

Dr. Leon Knopoff
University of California
Institute of Geophysics & Planetary
Physics
Los Angeles, CA 90024

Dr. Kenneth H. Olsen
Los Alamos Scientific Laboratory
Post Office Box 1663
Los Alamos, NM 87545

Prof. Jon F. Claerbout
Prof. Amos Nur
Dept. of Geophysics
Stanford University
Stanford, CA 94305 (2 copies)

Dr. Robert Burridge
Schlumberger-Doll Research Ctr.
Old Quarry Road
Ridgefield, CT 06877

Dr. Eduard Berg
Institute of Geophysics
University of Hawaii
Honolulu, HI 96822

Dr. Robert Phinney
Dr. F.A. Dahlen
Dept. of Geological & Geophysical Sci.
Princeton University
Princeton, NJ 08540 (2 copies)

Dr. Kin-Yip Chun
Geophysics Division
Physics Department
University of Toronto
Ontario, CANADA M5S 1A7

New England Research, Inc.
Attn: Dr. Randolph Martin III
P.O. Box 857
Norwich, VT 05055

Sandia National Laboratory
Attn: Dr. H.B. Durham
Albuquerque, NM 87185

Dr. Gary McCartor
Mission Research Corp.
735 State Street
P. O. Drawer 719
Santa Barbara, CA 93102

Dr. W. H. K. Lee
USGS
Office of Earthquakes, Volcanoes,
& Engineering
Branch of Seismology
345 Middlefield Rd
Menlo Park, CA 94025

AFGL/XO
Hanscom AFB, MA 01731-5000

AFGL/LW
Hanscom AFB, MA 01731-5000

AFGL/SULL
Research Library
Hanscom AFB, MA 01731-5000 (2 copies)

Secretary of the Air Force (SAFRD)
Washington, DC 20330

Office of the Secretary Defense
DDR & E
Washington, DC 20330

HQ DNA
Attn: Technical Library
Washington, DC 20305

Director, Technical Information
DARPA
1400 Wilson Blvd.
Arlington, VA 22209

Los Alamos Scientific Laboratory
Attn: Report Library
Post Office Box 1663
Los Alamos, NM 87544

Dr. Thomas Weaver
Los Alamos Scientific Laboratory
Los Alamos, NM 87544

Dr. Al Florence
SRI International
333 Ravenswood Avenue
Menlo Park, CA 94025-3493

END

7-87

DTIC